

Review

State of the Art of Lithium-Ion Battery SOC Estimation for Electrical Vehicles

Ruifeng Zhang ^{1,2,3,*} , Bizhong Xia ¹, Baohua Li ¹, Libo Cao ², Yongzhi Lai ³, Weiwei Zheng ³, Huawen Wang ³ and Wei Wang ³

¹ Graduate School at Shenzhen, Tsinghua University, Shenzhen 518055, China;
xiabz@sz.tsinghua.edu.cn (B.X.); libh@sz.tsinghua.edu.cn (B.L.)

² College of Mechanical and Vehicle Engineering, Hunan University, Changsha 410082, China; hdclb@163.com

³ Sunwoda Electronic Co., Ltd., Shenzhen 518108, China; lyz@sunwoda.com (Y.L.);
zhhw@sunwoda.com (W.Z.); wanghuawen@sunwoda.com (H.W.); willian-wang@sunwoda.com (W.W.)

* Correspondence: zrf223@126.com; Tel.: +86-188-9836-6838

Received: 16 June 2018; Accepted: 5 July 2018; Published: 11 July 2018



Abstract: State of charge (SOC) accurate estimation is one of the most important functions in a battery management system for battery packs used in electrical vehicles. This paper focuses on battery SOC estimation and its issues and challenges by exploring different existing estimation methodologies. The key technologies of lithium-ion battery state estimation methodologies of the electrical vehicles categorized under five groups, such as the conventional method, adaptive filter algorithm, learning algorithm, nonlinear observer, and the hybrid method, are explored in an in-depth analysis. Lithium-ion battery characteristic, battery model, estimation algorithm, and cell unbalancing are the most important factors that affect the accuracy and robustness of SOC estimation. Finally, this paper concludes with the challenges of SOC estimation and suggests other directions for possible research efforts.

Keywords: lithium-ion battery; state of charge; estimation algorithm; battery management system; electric vehicle

1. Introduction

The Nissan Altra EV was introduced as the first production lithium-ion battery electric vehicle in 1997 [1]. The goals for EVs are to operate at a temperature from -30 to $+52$ $^{\circ}\text{C}$ with a driving range of 300 miles per single charge and a use life of 15 years, according to the U.S. Advanced Battery Consortium (USABC) [2]. Implementation of rechargeable batteries for electrical vehicles (EVs) has become very popular because they can displace the consumption of fossil fuels and reduce the emissions of greenhouse gas [3]. Lithium-ion batteries are widely adopted due to their high energy and power density, high efficiency, high open-circuit cell voltage, broad temperature operating, and long lifespan [4].

In 1980, John Goodenough [5] created the first lithium-ion batteries, which use lithium cobalt oxide and lithium manganese dioxide as cathodes. Commercial lithium-ion batteries such as lithium cobalt oxide (LCO), lithium iron phosphate (LFP), lithium manganese oxide (LMO), lithium nickel manganese cobalt oxide (NMC), lithium nickel cobalt aluminum oxide (NCA), and lithium titanate oxide (LTO) have been widely accepted by electric vehicles in recent years [6]. According to USABC, today's lithium-ion batteries cannot meet the standards of EVs. At present, lots of scholars, scientists, and engineers are focusing on new battery research such as Li-O₂ batteries [2,7], lithium–sulfur batteries [8–14], lithium metal batteries [15,16], all-solid-state lithium batteries [17], al-ion batteries [18], fuel cells [19–22], supercapacitors [23,24], and so on. Electric vehicles require a high power and

high capacity for lithium-ion battery systems, thus demanding a battery management system to ensure a reliable and safe operation [25]. Additionally, a battery model is very important in states estimation of the model-based battery management system in EVs [26]. Haran [27] introduced a single particle model in order to develop a lumped structure. A physics-based model can predict microscopic behavior and performance, but requires a large computational power to solve the differential equations [28]. Equivalent circuit models (ECMs) have also been proposed to control-oriented purposes to estimate the electrical response and the amount of heat generation, which are frequently used to model cells due to their simplicity, the fact that their parameters are easy to obtain, and their real-time adaptability [28,29]. Various ECMs are now extensively used in EV studies, such as the Rint [30], Thevenin [31], The Partnership for a New Generation of Vehicles, (PNGV) [31], General nonlinear model (GNL) [32], and Resistance-Capacitance (RC)model [31]. In recent years, many new battery models have been put forward or improved, such as the fractional order PNGV model [33], invariant imbedding method [34], improved equivalent-circuit model [35], reduced order equivalent circuit battery models [36], fractional order impedance model [37–39], fuzzy model [40], kinetic battery model (KIBaM) [41], electrochemical/electrical-thermal coupled model [42], battery degradation model [42], and so on. The limitations of current battery technology include underutilization, capacity fade, thermal runaway, and stress-induced material damage [28].

In such a large number of models, the first step is to accurately identify the parameters of the model for battery state estimation. Two methods for battery model identification are electrochemical impedance spectroscopy (EIS) and pulse tests [43]. Because these methods rely on specific equipment for testing and processing large amounts of data, they are not suitable for online applications of electric vehicles. Therefore, some researchers have proposed recursive least squares (RLS) methods or adaptive filtering (AF) methods for on-line identification of battery model parameters [44]. Practice has proved that these methods are easier to implement in on-line applications. Besides, these methods can help to compensate for parameter values for battery variations and aging.

The state of the battery cell includes State of Charge (SOC) [45], State of Health (SOH) [46], State of Energy (SOE) [47–49], and State of Power (SOP) [35,50]. In order to estimate these states of batteries, the researchers need to put forward a new mathematical model or an algorithmic model besides the battery model mentioned above. The well-known techniques include the Kalman filter (KF) [51], extended Kalman filter (EKF) [52], unscented Kalman filter (UKF) [45], fading Kalman filter algorithm(FKF) [53], strong tracking cubature extended Kalman filter (STCEKF) [54], multirate strong tracking extended Kalman filter (MRSTEKF) [55], lazy extended Kalman filter (LEKF) [56], particle filter (PF) [57], sliding mode observer (SMO) [58–63], H-infinity observer [64–67], Luenberger observer [68], etc. The filter algorithms based on the equivalent circuit model with fixed model parameters are often used to estimate the battery state. However, the parameters of the equivalent circuit model are often affected by temperature, C-rate, SOC, and battery aging. Therefore, some joint-estimation methods have been proposed to handle these problems. These methods are usually made up of two parts. The first part is used to identify the parameters of the model with recursive least squares (RLS) on-line. The second part is used to estimate the battery state parameters with filter algorithms. Recently, because of the improvement of embedded hardware performance, some researchers have wanted to estimate battery state only using data, instead of using battery models. The Artificial Intelligence (AI) based learning approach including artificial neural network (ANN) modelling as well as the support vector machine (SVM) was proposed [69], and could be very accurate depending on the training data.

In order to make a perfect EV, scientists, academics, researchers, and engineers have performed much research to improve the accuracy of lithium-ion battery SOC estimation for EVs. In this paper, the SOC estimation approaches and shortcomings of the EV battery system are reviewed. This paper focuses on battery SOC estimation and its issues and challenges by exploring different existing estimation methodologies. At the beginning of the article, the lithium-ion battery characteristics of the EVs are reviewed. Following this, the common key technologies of battery state estimation are explored in an in-depth analysis. Besides, the various SOC issues and challenges are also discussed. At the

end of this article, the development direction of SOC is summarized. This review paper will be very helpful for scientists, academics, researchers, engineers, and automobile engineers and manufacturers for using the appropriate estimation method, which is especially important for the development of implementing a new battery management system or upgrading the battery management system in EVs in the future.

2. Lithium-Ion Battery

Lithium-Ion Battery

Compared with other materials, lithium ion batteries have the advantages of a high energy density, high power density, long cycle life, strong environmental adaptability, and high cell voltage. However, there are many kinds of lithium ion batteries, each of which has its own advantages, such as: LCO, which has an important specific energy; LMO, which has a high specific power; NCA and NMC, which are the cheaper lithium ion batteries and the most thermally stable; LFP, which has a flat OCV curve but a low capacity and high self-discharging rate; and LTO, which has a long lifespan and fast charge, but a low specific energy and higher cost [6]. Commercial lithium-ion batteries and their characteristics are shown in Table 1.

A spider chart for LIBs with various anode and cathode materials is shown in Figure 1. These batteries could be possible candidates use in EVs, because they could provide the possible performance needed for automotive applications. C-rate is the current value required for the battery to release its rated capacity within a specified time, which is equal to the multiple of the nominal capacity of the battery. One part of the important characteristic was to test the capacity loss after cycling at low and high C-rates while observing the heat generation during charging and discharging of the batteries. Moreover, the battery thermal stability, specific power, and specific energy were also compared.

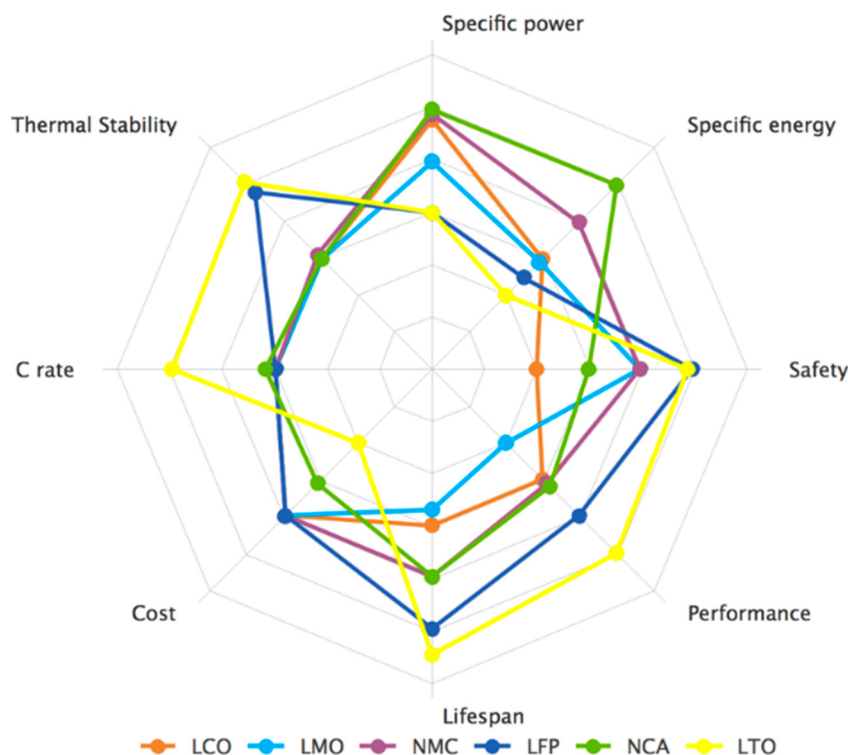


Figure 1. Spider chart for LIBs with various anode and cathode materials.

Table 1. Comparison of various commercial lithium-ion batteries [70].

Battery Name	Abbrev.	Year	Positive Electrode	Negative Electrode	Nominal Tension (V)	Specific Energy (Wh/kg)	Charge (C)	Discharge (C)	Lifespan	Thermal Runaway (°C)
Lithium cobalt oxide	LCO	since 1991	LiCoO ₂	Graphite	3.7~3.9	150~200	0.7~1	1	500~1000	150
Lithium nickel oxide	LNO	since 1996	LiNiO ₂	Graphite	3.6~3.7	150~200	0.7~1	1	>300	150
Lithium manganese oxide	LMO	since 1996	LiMn ₂ O ₄	Graphite	3.7~4.0	100~150	0.7~1	1	300~700	250
Lithium nickel manganese cobalt oxide	NMC	since 2008	Li(Ni _{0.33} Co _{0.33} Mn _{0.33})O ₂	Graphite	3.8~4.0	150~220	0.7~1	1	1000~2000	210
Lithium iron phosphate	LFP	since 1993	LiFePO ₄	Graphite	3.2~3.3	90~130	1	1	1000~2000	270
Lithium nickel cobalt aluminum oxide	NCA	since 1999	Li(Ni _{0.85} Co _{0.05} Al _{0.05})O ₂	Graphite	3.6~3.65	200~260	0.7	1	500	150
Lithium titanate	LTO	since 2008	LiMn ₂ O ₄ , Li(Ni _{0.85} Co _{0.05} Al _{0.05})O ₂	Li ₄ Ti ₅ O ₁₂	2.3~2.5	70~85	1	10	3000~7000	-

Figure 2 is a simplistic illustration for the safety operating window for a lithium-ion battery, which suggests that there is a safety window of cell temperature and voltage. The lithium-ion battery materials in a cell work best within a safe operating window that defines the safe temperature and voltage range, as well as the maximum current that the cell can accept during discharge and charging. According to Panchal's research, the decomposition of LiFePO₄ battery positive electrode and negative electrode materials is high [71,72]. When the temperature becomes higher, the positive material will start decomposing (LiCoO₂ will start decomposing at temperature of about 150 °C, LiNi_{0.8}Co_{0.15}Al_{0.05}O₂ at about 160 °C, LiNi_xCo_yMn_zO₂ at about 210 °C, LiMn₂O₄ at about 265 °C, and LiFePO₄ at about 310 °C) and produce oxygen. When the temperature is above 200 °C, the battery electrolyte will decompose and produce combustible gas [73]. Therefore, the heat management system is also very important in the battery system of electric vehicles. It is necessary to study the battery heat model and design a proper heating and cooling system for the battery [74].

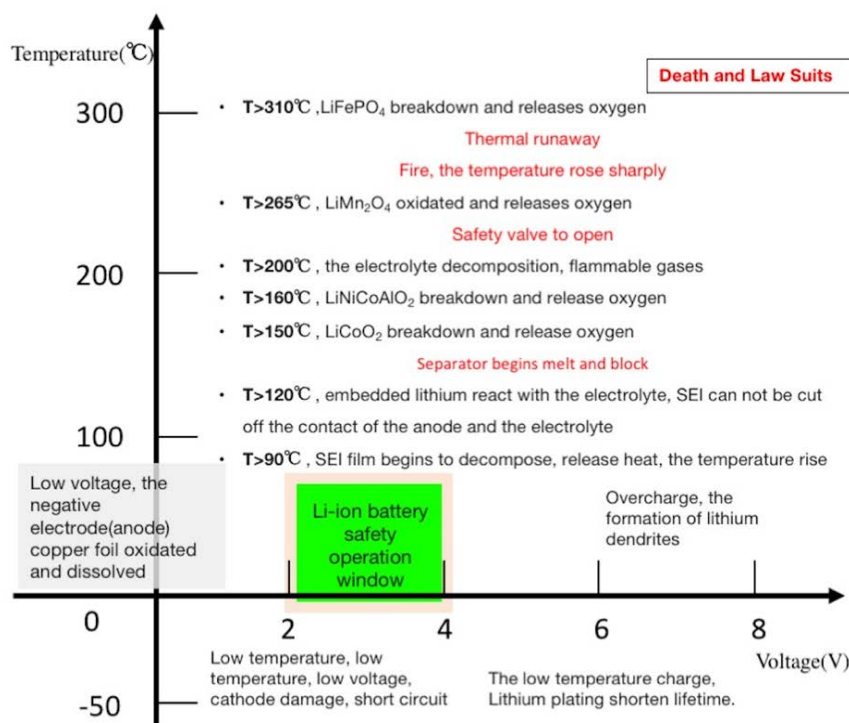


Figure 2. Safety operating window for a lithium-ion battery [73].

3. State of Charge Estimation Methods

Almost since the emergence of rechargeable batteries have systems that can indicate the available capacity value of the battery inside existed, such as the single-meter device invented by Heyer [75] in 1938. Curtis Instruments pioneered the development of gauges for monitoring the battery SOC of traction vehicles in 1963. Finger et al. [76] invented a battery current flowing integrator module in 1975. Peled [77] proposed a method based on predetermined voltage and temperature measurements relationship tables for the determination of lithium-ion batteries SOC in 1984. Aylor [78] presented a coulomb counting method for LA batteries. Gerard [79] developed an artificial neural network method for portable equipment battery state accurate estimation in 1997. Garche et al. [80] proposed a Kalman filters method to estimation SOC in 2000. KIM [60] presented the state equation for battery models and the systematic design approach for sliding mode observers in 2006. Tian [81] recently proposed the implementation of an SOC estimator for lithium-ion batteries in a field programmable gate array (FPGA). The most important points of the battery SOC estimation evolution are shown in Figure 3.

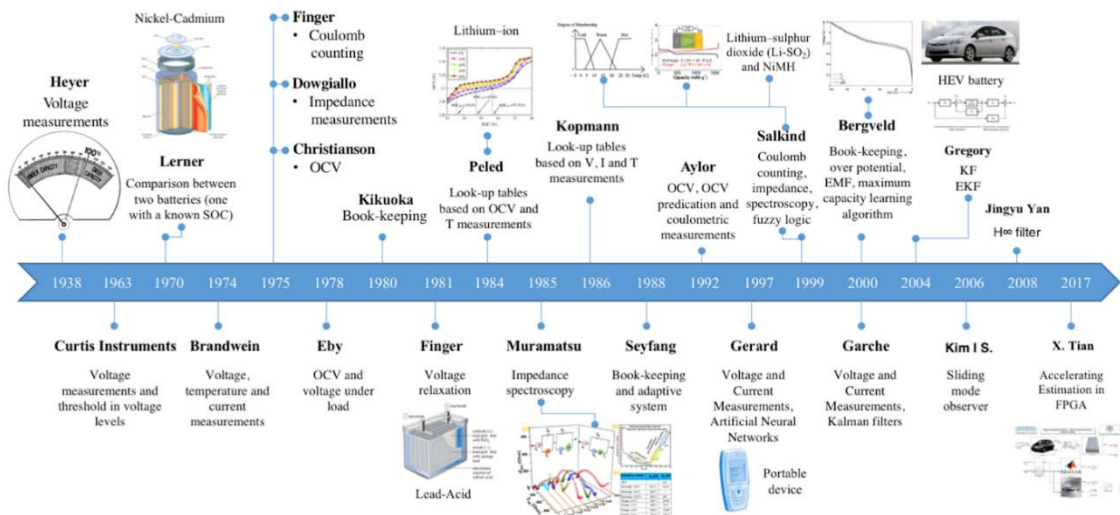


Figure 3. The most important points of the battery SOC estimation evolution.

According to the evolution history of battery SOC, it is known that when the rechargeable battery appears, research on the SOC also appears. Until now, the SOC is still the hot point and key point of research. The existing SOC estimation methodologies can also be categorized into five groups, which are the conventional method, the adaptive filter algorithm, the learning algorithm, the nonlinear observer, and the hybrid algorithm.

3.1. Conventional Method

The conventional method of SOC estimation consists of ampere-hour counting, the open circuit voltage (OCV) method, the impedance and internal resistance method, the electrochemical method, and the model-based method.

(1) Ampere-hour counting method

Ampere-hour counting is easy to implement with low computational complexity to estimate the SOC of a battery [4]. The Ampere-hour (Ah) counting estimation method is used to integrate the discharging or charging current to calculate the remaining charge in the battery, as follows [82]:

$$\text{SOC}(k) = \text{SOC}(0) - \frac{T}{C_n} \int_0^k (\eta \cdot I(t) - S_d) dt$$

where $\text{SOC}(0)$ is the battery initial SOC, $I(t)$ is the current at time t , T is the sampling period, C_n is the nominal capacity of the battery, η is the coulombic efficiency, and S_d is the self-discharging rate. For a LiFePo₄ battery, $\eta > 0.994$ under room temperature, the self-discharging rate is about 5% per month.

The biggest advantage of the Ah counting method is its low power computation cost, so it is widely used for battery SOC estimation. But the disadvantage of the Ah counting method is that it cannot remain accurate for a long time. The unknown initial SOC, capacity fading, self-discharge rate, and current sensor errors are the error sources for the Ah counting method. In order to improve the accuracy of the Ah method, the initial capacity and SOC value of the battery, and the current sensor drift can be corrected and adjusted regularly [83].

(2) OCV method

OCV is the method that uses the stable battery electromotive force in the open circuit state and SOC relationship to estimate the SOC value [83]. Although there is an approximate linear relationship between SOC and OCV, this relationship is not exactly the same for different batteries. It depends on the capacity and electrode material of the battery. For example, a lead-acid battery has a linear SOC and

OCV relationship, while a lithium-ion battery does not have this relationship [4]. LFP batteries have a very flat SOC-OCV relationship and a significant OCV hysteresis phenomenon. Thus, the OCV method is not reliable in LFP batteries [84]. Although the SOC-OCV relationship of lithium ion batteries is relatively stable, it will change according to the environmental temperature and cycle life of the battery. In addition, in order to have a reliable SOC-OCV relationship, researchers and engineers may need to conduct massive experiments at different temperatures and cycle lives [83].

Accurate SOC-OCV relationship data is the key issue for OCV method estimation depending on the fitting OCV relaxation model parameters [85]. However, the OCV voltage cannot be directly measured if there is no sufficient rest time. Direct use of the OCV method is employed to estimate SOC which has a very low power computation and a relatively high accuracy, but this method is limited by the working conditions. Therefore, it is generally used as a calibration auxiliary technology.

(3) Impedance and internal resistance method

The lithium-ion battery impedance and internal resistance can be used to describe the intrinsic electric characteristic under any current excitation, if temperature, SOC, and SOH are fixed. But it is very difficult to measure online electrical impedance spectroscopy (EIS), because sinusoidal alternating current (AC) may be required, the SOC and impedance relationship is not stable, and the cost is expensive [83]. To obtain the internal resistance, it needs direct current (DC) and the value of the voltage and current at a small time interval. However, internal resistance changes slowly and is hard to observe for SOC estimation. In general, SOC estimation based on the impedance and internal resistance method is not suitable for use in EVs [83].

(4) Electrochemical method

Estimating the amount of Li or the average Li concentration in the positive or negative electrodes is critical for SOC estimation based on the electrochemical model with partial differential equations. The SOC can be directly calculated from Li amount identification in the negative or positive electrodes of the electrochemical model. Nevertheless, the solution of partial differential equations is always too complex for online applications [83]. Generally speaking, the electrochemical model can theoretically obtain the most accurate SOC estimation. But, this model is only suitable for off-line design and performance analysis for lithium-ion batteries. Nevertheless, due to the complexity of the electrochemical model and the dozens of parameters of the battery model, this method is too difficult to use for online SOC estimation [83].

(5) Model-based method

In the conventional method, the above methods are not unsatisfactory for online SOC values. In order to achieve an accurate online SOC value, the battery models need to be developed. The most common usage of battery models includes the electrochemical model and equivalent circuit model (ECMs). ECMs mainly use resistances and RCs to simulate the electrical characteristics for lithium-ion batteries. An ideal ECM should be able to simulate the actual battery voltage under any current excitation. However, some characteristics of the lithium-ion batteries cannot be well represented by circuit elements, such as the hysteresis effect or the Warburg effect. Therefore, pure mathematical models with hysteresis are used to further improve the accuracy of voltage simulation [83].

Two technical routes are usually used to estimate SOC using ECM. The first method is a simple way to estimate SOC directly through ECM parameter identification. The second method firstly uses a predetermined SOC to realize OCV and then estimates the lithium-ion battery voltage through ECM. Hence, the SOC-OCV relationship is very important not only in OCV method estimation, but also in model-based method estimation [83].

3.2. Adaptive Filter Algorithm

In order to improve the accuracy and robustness of the battery SOC estimation and reduce the noise influence on the battery model, the adaptive filtering algorithm of modern control theory provides another method for estimating the SOC. Figure 4 shows the flow chart of the adaptive filter algorithm based on the modern control theory. As suggested in the flow chart, there are three basic functions that need to be discussed. The first is how to use the battery SOC model to estimate a predetermined SOC as an input for the models. The second is which model should calculate the battery voltage at the predetermined SOC as an output for the models. The third is how to calculate the gain to update the SOC by comparing the measured voltage and model voltage.

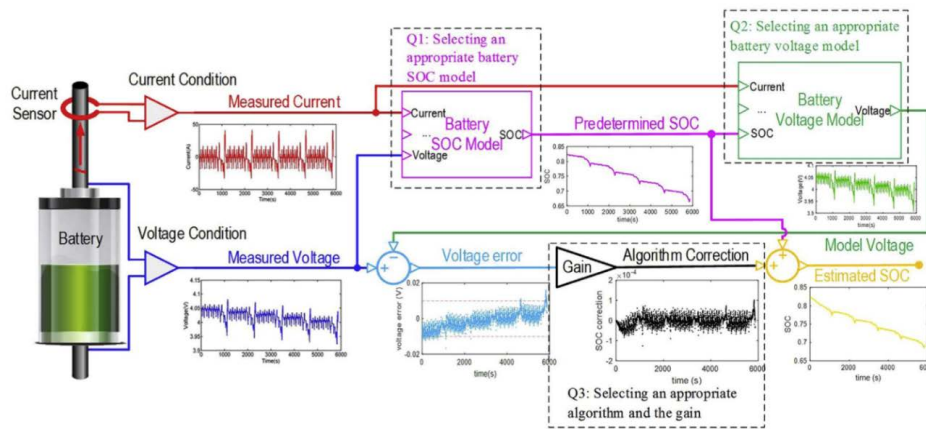


Figure 4. Flow chart of the adaptive filter algorithm of the modern control theory-based SOC estimation [83].

(1) Kalman filter

The Kalman filter is the optimum state estimator and intelligent tool for a linear system, and is often used to estimate the battery dynamic state, such as that described in [4,51]. The most attractive feature of KF is that it has a self-correcting nature when the system is running, which helps to tolerate high variations. The Kalman filter algorithm is shown in Table 2. The KF linear state-space model includes the process of predicting the current state from the earlier state and a measurement which updates the current state to converge it to the real value.

Table 2. Kalman filter algorithm [51].

Linear state-space model
$x_{k+1} = A_k x_k + B_k u_k + w_k$
$y_k = C_k x_k + D_k u_k + v_k$
Initialization
For $k = 0$, set
$\hat{x}_0^+ = \mathbb{E}[x_0]$
$P_{\hat{x},0}^+ = \mathbb{E}[(x_0 - \hat{x}_0^+)(x_0 - \hat{x}_0^+)^T]$
Computation
For $k = 1, 2, \dots$ compute
State estimate time update : $\hat{x}_0^- = A_{k-1} \hat{x}_{k-1}^+ + B_{k-1} u_{k-1}$
Error covariance time update : $P_{\hat{x},0}^- = A_{k-1} P_{\hat{x},0}^+ A_{k-1}^T + Q_w$
Kalman gain matrix : $K_k = P_{\hat{x},k}^- C_k^T [C_k P_{\hat{x},0}^- C_k^T + R_v]^T$
State estimate measurement update:
$\hat{x}_k^+ = \hat{x}_0^- + K_k [y_k - C_k \hat{x}_0^- - D_k u_k]$
Error covariance measurement update:
$P_{\hat{x},k}^+ = (I - K_k C_k) P_{\hat{x},0}^-$

According to Ting and Yatsui's [86,87] research, researchers should use the KF method and combine the open-circuit voltage and Ah counting to compensate for the non-ideal factors that can prolong the operation of the battery. The advantage of the KF method is that it can accurately estimate the states affected by external disturbances. Nonetheless, KF cannot be directly applied to the state prediction of a nonlinear system and it requires complex calculations [4,88].

(2) Extended Kalman filter

If the system is nonlinear, then we can use a linearization process at each time step to approximate the nonlinear system with a linear time varying (LTV) system. Then, the system is applied to the Kalman filter, resulting in an extended Kalman filter (EKF) on the true nonlinear system applied for the SOC estimation [44,51,52,82,89–95].

EKF linearized the battery model using partial derivatives and first order Taylor series expansion. The state-space model is linearized at each time instance, which compares the predicted value with its measured batteries terminal voltage to correct the estimation parameters for SOC. However, if the system is highly non-linear, linearization error may occur due to the lack of accuracy in the first order Taylor series under a highly non-linear condition [4]. The extended Kalman filter algorithm is shown in Table 3.

Table 3. Summary of the extended Kalman filter algorithm [51].

Nonlinear state-space model
$x_{k+1} = f(x_k, u_k) + w_k$
$y_k = g(x_k, u_k) + v_k$
Definitions
$\hat{A}_k = \frac{\partial f(x_k, u_k)}{\partial x_k} \Big _{x_k=\hat{x}_k^+}, \hat{C}_k = \frac{\partial g(x_k, u_k)}{\partial x_k} \Big _{x_k=\hat{x}_k^-}$
Initialization
For $k = 0$, set
$\hat{x}_0^+ = \mathbb{E}[x_0]$
$P_{\hat{x},0}^+ = \mathbb{E}[(x_0 - \hat{x}_0^+)(x_0 - \hat{x}_0^+)^T]$
Computation
For $k = 1, 2, \dots$ compute
State estimate time update : $\hat{x}_k^- = f(\hat{x}_{k-1}^+, u_{k-1})$
Error covariance time update : $P_{\hat{x},k}^- = \hat{A}_{k-1} P_{\hat{x},k-1}^+ \hat{A}_{k-1}^T + Q_w$
Kalman gain matrix : $K_k = P_{\hat{x},k}^- \hat{C}_k^T [\hat{C}_k P_{\hat{x},k}^- \hat{C}_k^T + R_v]^T$
State estimate measurement update:
$\hat{x}_k^+ = \hat{x}_k^- + K_k[y_k - g(\hat{x}_k^-, u_k)]$
Error covariance measurement update:
$P_{\hat{x},k}^+ = (I - K_k \hat{C}_k) P_{\hat{x},k}^-$

Because of the advantages of EKF, many researchers have applied this method to the study of battery SOC, such as Lee et al. [96], who proposed dual EKF, and Chen et al. [97] and Zhu et al. [98], who improved the nonlinear battery model with EKF to estimate the SOC of a lithium-ion battery. Compared to other extended Kalman filter algorithms, the strong tracking cubature extended Kalman filter (STCEKF) proposed by Gao et al. [54] gave an accurate SOC prediction and faster computational time. J. Jia et al. [55] proposed a multirate strong tracking extended Kalman filter (MRSTEKF) by introducing the multirate control strategy and lifting technology into a strong tracking extended Kalman filter (STEKF) to improve the tracking stability and estimation precision of SOC. Result shows that the MRSTEKF is faster than EKF and STEKF by 55.34% and 49.51%, and is more precise by 52.66%

and 33.88%, respectively [55]. The advanced EKF method has a better performance than generality EKF, KF, and the ampere-hour counting method in terms of effectiveness and dynamic adaptability [96–98].

(3) Adaptive extended Kalman filter

An adaptive extended Kalman filter (AEKF) is proposed in [95] using a modified second-order RC network-based battery model and automatic correction of the process noise matrix and measurement noise matrix to obtain a correct and robust lithium-ion battery. A summary of the adaptive extended Kalman filter algorithm is shown in Table 4.

Table 4. Summary of the adaptive extended Kalman filter algorithm [99].

Nonlinear state-space model	$x_{k+1} = f(x_k, u_k) + w_k$
	$y_k = g(x_k, u_k) + v_k$
Definitions	$\hat{A}_k = \frac{\partial f(x_k, u_k)}{\partial x_k} \Big _{x_k=\hat{x}_k^+}, \hat{C}_k = \frac{\partial g(x_k, u_k)}{\partial x_k} \Big _{x_k=\hat{x}_k^-}$
Initialization	
For $k = 0$, set	$\hat{x}_0^+ = \mathbb{E}[x_0]$
	$P_{\tilde{x},0}^+ = \mathbb{E}[(x_0 - \hat{x}_0^+)(x_0 - \hat{x}_0^+)^T]$
Computation	
For $k = 1, 2, \dots$ compute	
State estimate time update :	$\hat{x}_k^- = f(\hat{x}_{k-1}^+, u_{k-1})$
Error covariance time update :	$P_{\tilde{x},k}^- = \hat{A}_{k-1} P_{\tilde{x},k-1}^+ \hat{A}_{k-1}^T + Q_{k-1}$
Kalman gain matrix :	$K_k = P_{\tilde{x},k}^- \hat{C}_k^T [\hat{C}_k P_{\tilde{x},k}^- \hat{C}_k^T + R_{k-1}]^{-1}$
State estimate measurement update:	$\hat{x}_k^+ = \hat{x}_k^- + K_k [y_k - g(\hat{x}_k^-, u_k)]$
Error covariance measurement update:	$P_{\tilde{x},k}^+ = (I - K_k \hat{C}_k) P_{\tilde{x},k}^-$
For $k \geq N$, compute	
Residual sequence :	$v_k = y_k - g(\hat{x}_k^+, u_k)$
Estimated variance – covariance of residual sequence :	$\hat{\mu}_k = \frac{1}{N} \sum_{j=k-N+1}^k v_j v_j^T$
Process noise matrix update :	$Q_k = K_k \hat{\mu}_k K_k^T$
Measurement noise matrix update :	$R_k = \hat{\mu}_k + C_k P_{\tilde{x},k}^+ C_k^T$

Xiong et al. [100] built an online AEKF algorithm with the Thevenin model to estimate SOC. This AEKF algorithm can reduce the SOC estimation error by 2%, validated by an urban dynamometer driving schedule (UDDS). It shows that AEKF is better than EKF in regard to accuracy and reliability.

(4) Fading Kalman filter

The Fading Kalman filter (FKF) is insensitive to noise covariance variations and capable of compensating for any modeling error, because it uses a fading factor that can limit its memory. The Fading Kalman filter algorithm is shown in Table 5.

Table 5. Summary of the Fading Kalman filter algorithm [53].

Linear state-space model
$x_{k+1} = A_k x_k + B_k u_k + w_k$
$y_k = C_k x_k + D_k u_k + v_k$
Initialization
For $k = 0$, set
$\hat{x}_0^+ = \mathbb{E}[x_0]$
$P_{\hat{x},0}^+ = \mathbb{E}[(x_0 - \hat{x}_0^+)(x_0 - \hat{x}_0^+)^T]$
Computation
For $k = 1, 2, \dots$ compute
State estimate time update : $\hat{x}_k^- = A_{k-1} \hat{x}_{k-1}^+ + B_{k-1} u_{k-1}$
Error covariance time update : $P_{\hat{x},0}^- = A_{k-1} \alpha P_{\hat{x},0}^+ A_{k-1}^T + Q_k$
Kalman gain matrix : $K_k = P_{\hat{x},k}^- C_k^T [C_k P_{\hat{x},0}^- C_k^T + R_k]^{-1}$
State estimate measurement update:
$\hat{x}_k^+ = \hat{x}_k^- + K_k [y_k - C_k \hat{x}_k^- - D_k u_k]$
Error covariance measurement update:
$P_{\hat{x},k}^+ = (I - K_k C_k) P_{\hat{x},k}^-$

KaiChin Lim et al. [53] proposed an FKF to estimate the OCV and SOC. According to this study, FKF can avoid the possibility of large estimation errors, which may occur when using the traditional Kalman filter because of its capability to compensate for any modeling error through a fading factor. The advantage of the Fading Kalman filter is that it can provide the feasibility and simplicity required for real-time application with highly precise SOC estimation [53].

(5) Unscented Kalman filtering

The EKF method is good at the first and second order of a non-linear model, but is bad at a highly non-linear state-space model. The Unscented Kalman filtering (UKF) algorithm is used to handle this problem [83]. UKF is an updated version of EKF that applies a discrete-time filtering algorithm and unscented transform to solve filtering problems. UKF based on unscented transformation was proposed to avoid the weakness of Taylor series expansion compared to EKF [45,92,101]. The UKF approach for SOC estimation is shown in Table 6.

Table 6. Summary of the Unscented Kalman filter approach for SOC estimation [102].

Non-linear state-space model
$x_{k+1} = f(x_k, u_k) + w_k$
$y_k = g(x_k, u_k) + v_k$
Initialization
Measure ambient temperature, prepare $U_{OCV}(SOC, T)$ and R_0, C_0
Initial guess : S_0
Covariance matrix : P_0
Process and measurement noise covariance : Σ_{w_0}, Σ_v
Computation
For $k = 1, 2, \dots$ compute
Generate sigma points at time $k - 1$, ($k \in [1, \dots, \infty]$)
$\chi_{k-1} = \begin{bmatrix} S_{k-1} \\ R_{k-1} \end{bmatrix} = [\bar{\chi}_{k-1}, \bar{\chi}_{k-1} + \sqrt{(n + \lambda) P_{k-1}}, \bar{\chi}_{k-1} - \sqrt{(n + \lambda) P_{k-1}}]$
Predict the prior state mean and covariance
Calculate sigma points through state function:
$\chi_{k k-1}^i = \begin{bmatrix} S_{k k-1}^i \\ R_{k k-1}^i \end{bmatrix} = \begin{bmatrix} S_{k-1}^i - \frac{I_{k-1} \times \Delta t}{C_n} \\ R_{k-1}^i \end{bmatrix}, i = 1, \dots, 2n$

Table 6. Cont.

Calculate the prior mean and covariance:
$\hat{x}_k^- = \sum_{i=0}^{2n} w_m^i \chi_{k k-1}^i, P_k^- = \sum_{i=0}^{2n} w_c^i [\chi_{k k-1}^i - \hat{x}_k^-] [\chi_{k k-1}^i - \hat{x}_k^-]^T + \Sigma_w$
Update using the measurement function
Calculate the sigma points : $y_{k k-1} = U_{OCV}(\text{SOC}_{k k-1}, T) - I_k \times R(T)_k + C(T)$
Calculate the propagated mean : $\hat{y}_k^- = \sum_{i=0}^{2n} w_m^i y_{k k-1}^i$
Calculate the covariance of the measurement:
$P_{y_k^-, y_k^-} = \sum_{i=0}^{2n} w_c^i [y_{k k-1}^i - \hat{y}_k^-] [y_{k k-1}^i - \hat{y}_k^-]^T + \Sigma_v$
Calculate the cross-covariance and the state and measurement:
$P_{x_k^-, y_k^-} = \sum_{i=0}^{2n} w_c^i [\chi_{k k-1}^i - \hat{x}_k^-] [y_{k k-1}^i - \hat{y}_k^-]^T$
Compute filter gain and update and achieve the posterior SOC estimation
Compute the filter gain : $K_k = P_{x_k^-, y_k^-} P_{y_k^-, y_k^-}^{-1}$
Update the posterior state mean : $S_k^+ = S_k^- + K_k (y_k - \hat{y}_k^-)$
Update the posterior covariance : $P_k = P_k^- + K_k P_{y_k^-, y_k^-} K_k^T$

(6) Sigma-point Kalman filter

The sigma-point Kalman filter (SPKF) is another method for the estimation of the states in the non-linear system. SPKF depends on numeric approximations instead of EKF analytic approximations [103,104]. The algorithm selects sets of sigma points, which is completely similar to the value of mean and covariance of the model being developed. The sigma-point Kalman filter approach for SOC estimation is shown in Table 7.

Table 7. Summary of the sigma-point Kalman filter for SOC estimation [103,104].

Non-linear state-space model
$x_k = f(x_{k-1}, u_{k-1}, w_{k-1}, k-1)$
$y_k = g(x_k, u_k, v_k, k)$
Definitions: let
$x_k^a = [x_k^T, w_k^T, v_k^T]^T, \chi_k^a = [(\chi_k^x)^T, (\chi_k^w)^T, (\chi_k^v)^T]^T, p = 2 \times \dim(x_k^a)$
Initialization
For $k = 0$, set
$\hat{x}_0^+ = \mathbb{E}[x_0]$
$\hat{x}_0^{a,+} = \mathbb{E}[x_0^a] = [(\hat{x}_0^+)^T, \bar{w}, \bar{v}]^T$
$P_{\hat{x},0}^+ = \mathbb{E}[(x_0 - \hat{x}_0^+)(x_0 - \hat{x}_0^+)^T]$
$P_{\hat{x},0}^{a,+} = \mathbb{E}[(x_0^a - \hat{x}_0^{a,+})(x_0^a - \hat{x}_0^{a,+})^T] = \text{diag}(P_{\hat{x},0}^+, P_w, P_v)$
Computation
For $k = 1, 2, \dots$ compute
State estimate time update
$\chi_{k-1}^{a,+} = \left\{ \hat{x}_{k-1}^{a,+}, \hat{x}_{k-1}^{a,+} + \gamma \sqrt{P_{\hat{x},k-1}^{a,+}}, \hat{x}_{k-1}^{a,+} - \gamma \sqrt{P_{\hat{x},k-1}^{a,+}} \right\}$
$\chi_{k,i}^{x,-} = f(\chi_{k-1,i}^{x,+}, u_{k-1}, \chi_{k-1,i}^{w,-}, k-1)$
$\hat{x}_k^- = \sum_{i=0}^p \alpha_i^{(m)} \chi_{k,i}^{x,-}$
Error covariance time update
$P_{\hat{x},k}^- = \sum_{i=0}^p \alpha_i^{(c)} (\chi_{k,i}^{x,-} - \hat{x}_k^-) (\chi_{k,i}^{x,-} - \hat{x}_k^-)^T$
Output estimate
$\mathcal{Y}_{k,i} = g(\chi_{k,i}^{x,-}, u_k, \chi_{k-1,i}^{w,+}, k)$
$\hat{y}_k = \sum_{i=0}^p \alpha_i^{(m)} \mathcal{Y}_{k,i}$

Table 7. Cont.

Estimator gain matrix
$P_{\tilde{x},k} = \sum_{i=0}^p \alpha_i^{(c)} (\mathcal{Y}_{k,i} - \hat{y}_k) (\mathcal{Y}_{k,i} - \hat{y}_k)^T$
$P_{\tilde{x}\tilde{y},k}^- = \sum_{i=0}^p \alpha_i^{(c)} (\chi_{k,i}^{x,-} - \hat{x}_k^-) (\mathcal{Y}_{k,i} - \hat{y}_k)^T$
$K_k = P_{\tilde{x}\tilde{y},k} P_{\tilde{x}\tilde{y},k}^{-1}$
State estimate measurement update
$\hat{x}_k^+ = \hat{x}_k^- + K_k (y_{k,i} - \hat{y}_k)$
Error covariance measurement update
$P_{\tilde{x},k}^- = P_{\tilde{x},k}^- - K_k P_{\tilde{y},k}^- K_k^T$

He et al. [105] proposed a joint battery model and SOC estimation method based on the sigma point Kalman filter. These reports show that the proposed combinatorial method only requires a very small computational load and less memory storage to achieve effective results.

The advantages of using SPKF are that it has an identical calculation complexity to EKF without considering Jacobian matrices. In SPKF, derivatives do not need to be calculated, the original functions do not need to be differentiable, and the computational complexity is the same order as EKF, so the gains are made at little or no additional cost and are theoretically more precise than EKF [103].

(7) Particle Filter (PF)

The Particle filter (PF) algorithm is used to estimate the states, which approximate the probability density function of a non-linear system by using the Monte Carlo simulation technique [4]. Ruifeng Zhang et al. [106] proposed a cubature particle filter (CPF) for accurate and reliable SOC estimation. Min Ye [107] proposed double-scale dual particle filtering (D-PF) and a double-scale dual adaptive particle filter (D-APF) for SOC estimation. However, the particle filter method has a higher computation. The double-scale dual adaptive particle filter approach for SOC estimation is shown in Table 8.

Table 8. Summary of the double-scale dual adaptive particle filter for SOC estimation [107].

Non-linear state-space model
$x_k = f(x_{1,k-1}, u_{k-1}, \theta_{l-1}) + w_{1,k-1}$
$\theta_l = \theta_{l-1} + w_{2,l-1}$
$y_k = g(x_{2,k-1}, u_{k-1}, \theta_{l-1}) + v_{k-1}$
Initialization
$k, j = 0, l = 0$
Randomly generate N initial particles $x_0^i (i = 1, 2, \dots, N)$ for the state and initial particles $\theta_0^i (i = 1, 2, \dots, M)$ for the parameter, and give an initial weight for every particle. Set the maximum and minimum noise variances of each state.
State estimation
For $k = 1, 2, \dots$ compute
Weight coefficient sampling : The weight coefficient of every particle is selected as follows :
$w_{1,k}^i = \frac{1}{\sqrt{2\pi R_1}} \exp \left\{ -\frac{(y_k - y_k^i)^2}{2R_1} \right\}$
Normalize the weight coefficients as follows : $w_{1,k}^i = \frac{w_{1,k}^i}{\sum_{i=1}^N w_{1,k}^i}$
State estimation : $\hat{x}_k = \sum_{i=1}^N w_{1,k}^i x_k^i$
Evaluate the effective sample size : $N_{eff1} = \frac{1}{\sum_{i=1}^N (w_{1,k}^i)^2}$ to evaluate the necessity or re-sampling
Parameter estimation (if $k \% L == 1$)
For $l = l + 1$ compute
Weight coefficient sampling : The weight coefficient of every particle is selected as follows :
$w_{2,l}^j = \frac{1}{\sqrt{2\pi R_2}} \exp \left\{ -\frac{(y_k - y_k^j)^2}{2R_2} \right\}$

Table 8. Cont.

Normalize the importance of the weights as follows : $w_{2,l}^j = \frac{w_{2,l}^j}{\sum_{j=1}^M w_{2,l}^j}$
Parameter estimation : $\hat{\theta}_l = \sum_{j=1}^M w_{2,l}^j \theta_l^j$
Evaluate the effective sample size : $Neff_2 = \frac{1}{\sum_{j=1}^M (w_{2,l}^j)^2}$ to evaluate the necessity or re-sampling
Noise variance update for dual adaptive particle filter
Compute the demand value of the noise variance:
$e_{x,k} = \frac{1}{W} \sum_{i=1}^W \hat{x}_k - f(\hat{x}_{i-1}, u_{i-1}, \theta_{k-1}) $
$e_{\theta,l} = \frac{1}{W} \sum_{i=1}^W \hat{\theta}_l - \hat{\theta}_{l-1} $
Noise variance update:
$\sigma_{a,k} = \begin{cases} \min(e_{a,k}, \sigma_{a,max}) & \text{if } e_{a,k} > \sigma_{a,k-1} \\ \max(\beta \sigma_{a,k-1}, \sigma_{a,min}) & \text{if } e_{a,k} \leq \sigma_{a,k-1} \end{cases}$
$\sigma_{b,l} = \begin{cases} \min(e_{b,l}, \sigma_{b,max}) & \text{if } e_{b,l} > \sigma_{b,l-1} \\ \max(\beta \sigma_{b,l-1}, \sigma_{b,min}) & \text{if } e_{b,l} \leq \sigma_{b,l-1} \end{cases}$

(8) $H\infty$ filter

The $H\infty$ filter is a simple design model with a strong robustness under certain conditions. However, hysteresis, aging, and temperature effects may deviate the accuracy of the model [4]. Charkhgard et al. [108] proposed a universal linear model using an adaptive $H\infty$ filter (AHF) to estimate SOC and compared it with the adaptive extended Kalman filter and square-root unscented Kalman filter. The adaptive $H\infty$ filter for SOC estimation is shown in Table 9.

Particle filter and observer methods can further improve the quality of the feedback gain, leading to better SOC estimation. However, the particle filter and observer method have a higher computational complexity compared to the Kalman filter method.

Table 9. Summary of the adaptive $H\infty$ filter for SOC estimation [108].

State-space model
$x_{k+1} = A_k x_k + B_k u_k + w_k$
$y_k = C_k x_k + D_k u_k + v_k$
$\zeta_k = L_k x_k$
Definitions:
$A_k \triangleq A(\hat{x}_k), B_k \triangleq B(\hat{x}_k), C_k \triangleq C(\hat{x}_k^-), D_k \triangleq D(\hat{x}_k^-),$
Initialization
For $k = 0$, set
$\hat{x}_0^+ = \mathbb{E}[x_0]$
$P_{\hat{x},0}^+ = \hat{R}_{\hat{x},0}^+ = \hat{Q}_{\hat{x},0}^+ = \epsilon I, \epsilon \ll 1$
Computation
For $k = 1, 2, \dots$ compute
State estimate time update : $\hat{x}_k^- = A_{k-1} \hat{x}_{k-1}^+ + B_{k-1} u_{k-1}$
Error covariance time update : $P_{\hat{x},k}^- = A_{k-1} P_{\hat{x},k}^+ A_{k-1}^T + \hat{Q}_{k-1}$
Kalman gain matrix:
$\gamma_{ok} = \alpha \sqrt{\bar{\sigma}(P_{\hat{x},k}^-)}, \alpha > 1$
$R_{e,k} = \begin{bmatrix} \hat{R}_{k-1} & 0 \\ 0 & -\gamma_{ok}^2 I \end{bmatrix} + \begin{bmatrix} C_k \\ L_k \end{bmatrix} P_{\hat{x},k}^+ \begin{bmatrix} C_k^T & L_k^T \end{bmatrix}$
$K_k = P_{\hat{x},k}^- \begin{bmatrix} C_k^T & L_k^T \end{bmatrix} R_{e,k}^{-1}$
$K_{s,k} = P_{\hat{x},k}^- C_k^T [C_k P_{\hat{x},k}^- C_k^T + \hat{R}_{k-1}]^{-1}$

Table 9. Cont.

State estimate measurement update: $\hat{x}_k^+ = \hat{x}_k^- + K_{s,k}[y_k - C_k \hat{x}_k^- - D_k u_k]$ $\hat{\zeta}_k = L_k \hat{x}_k^+$
Error covariance measurement update: $P_{\hat{x},k}^+ = (I - K_k \begin{bmatrix} C_k \\ L_k \end{bmatrix}) P_{\hat{x},k}^-$
Adjusting weighing matrices: $v_j^+ = y_j - (C_j \hat{x}_j^- - D_j u_j)$ $\hat{R}_{\hat{x},k}^+ = \frac{1}{N} \sum_{j=k-N+1}^k [v_j^+ v_j^{+T} - C_j P_{\hat{x},j}^+ C_j^T]$ $\hat{Q}_{\hat{x},k}^+ = \frac{1}{N} \sum_{j=k-N+1}^k [K_{s,k} v_k v_j^T K_{s,j}^T + P_{\hat{x},j}^+ - A_{j-1} P_{\hat{x},j-1}^+ A_{j-1}^T]$

In the summary of the SOC estimation method based on modern control theory, using the Ah counting method, ECM, and the EKF algorithm, this estimation method could be quite reliable, with an acceptable computational complexity for online applications. Therefore, it has become a widely studied and implemented battery SOC estimation method.

3.3. Learning Algorithm

(1) Artificial Neural Network (ANN)

The artificial neural network (ANN) has the self-learning skills and adaptability to demonstrate a complex non-linear model. ANN can use the training data to estimate SOC without knowing information about the internal structure of the battery and initial SOC information. Generally, at least three layers are used for the formation of an ANN algorithm, including an input layer, one or more hidden layers, and an output layer. The structure of ANN for estimating SOC is shown in Figure 5.

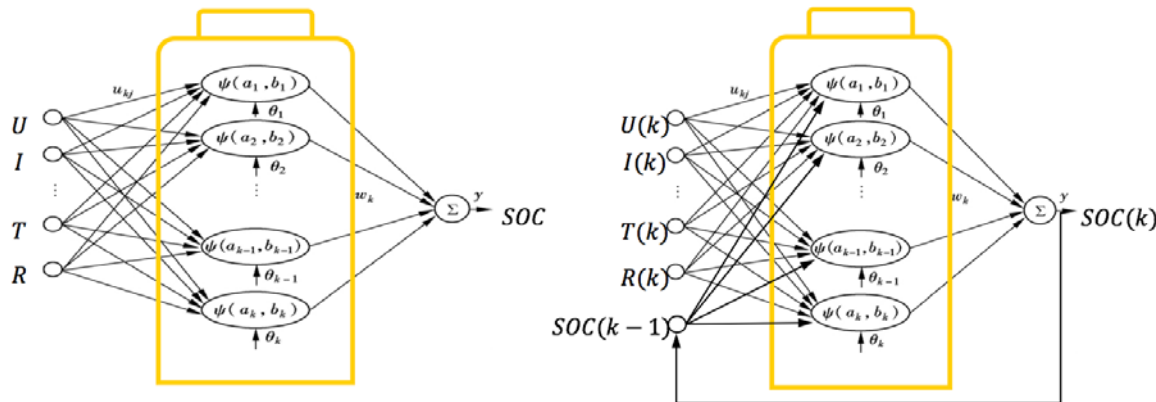


Figure 5. The complete structure of ANN for estimating SOC [109].

Usually, the ANN method uses the lithium-ion battery terminal voltage, discharge or charge current, and ambient temperature as the input and SOC as the output. Ruifeng and Cui et al. [109] proposed the Levenberg-Marquardt (L-M) algorithm optimized multi-hidden-layer wavelet neural network (WNN) for SOC estimation. Xuanju Dang et al. [110] proposed the dual neural network fusion battery model for SOC estimation. Shijie Tong et al. [111] proposed a new architecture for SOC estimation using a load-classifying neural network and yielded a 3.8% average estimation error. This method has a simpler model training procedure, broader choice of training data, and smaller computational cost. Hicham Chaoui et al. [112] proposed an SOC and SOH estimation based on the input time-delayed neural network (ITDNN) that accounts for both aging and temperature effects.

This technique uses the multi-layer perceptron structure with the back-propagation (BP) learning rule to adjust the intra-neuron connecting weights to yield accurate results.

The advantage of the ANN method is that it can operate in non-linear conditions. Nevertheless, the algorithm needs to store large amounts of training data, which not only requires a super computing power but also large memory storage in the whole system.

(2) Support Vector Machine (SVM)

SVM is the method that uses the regression algorithm to transform a lower dimension model into a high dimension linear model [4]. SVM was first designed to solve the nonlinear two-class classification problem [113]. The key point of SVM is to map the original sample from the low dimensional space to high dimensional space so that a linear hyperplane can be found to separate samples from two classes, as shown in Figure 6.

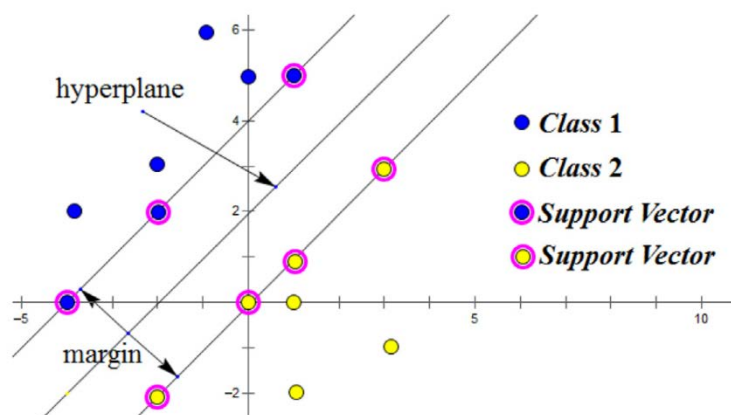


Figure 6. Hyperplan to separate samples from two classes [113].

Hanmin Sheng et al. [114] proposed an SOC estimation method based on the fuzzy least square support vector machine. J.N. Hu et al. [113] proposed an SOC estimation based on an optimized SVM for regression with a double search optimization process.

SVM architecture is simple and elegant, which used in the SOC estimation is time-consuming. Moreover, it can have the ability to tolerate noise and be scalable to integrate knowledge from other indicators such as temperature, power, etc.

(3) Extreme Machine Learning (ELM)

There are different ELM methods such as online-sequential ELM(OS-ELM), parallel chaos search ELM(P-ELM), incremental-ELM(I-ELM), bidirectional-ELM(B-ELM), and the proposed adaptive online-sequential ELM(AOS-ELM) that have been used to estimate the SOC of batteries in recent year [113]. For example, Cheng Siong Chin et al. [113] proposed an adaptive online sequential extreme learning machine (AOS-ELM) to estimate the battery SOC at different ambient temperatures. According to the research, the ELM method can reduce the error and produce a faster computational time. An example of ELM architecture is shown in Figure 7.

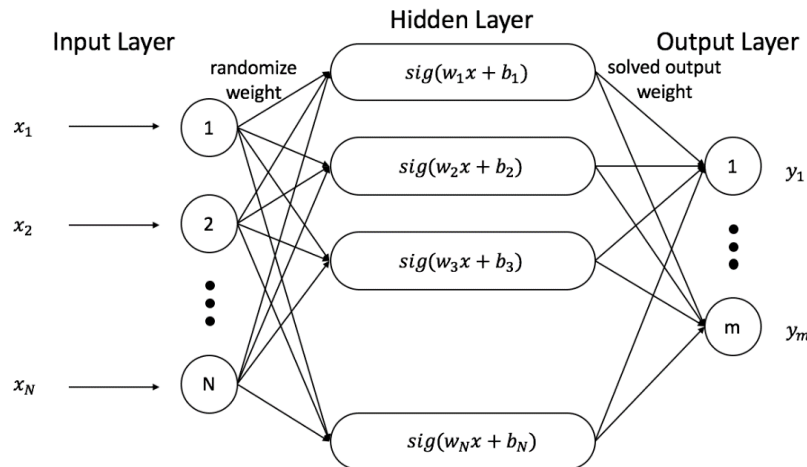


Figure 7. An example of ELM architecture [115].

(4) Genetic Algorithm (GA)

GA is an inspiration of the biological genetic process to find approximate optimal solutions. Its basic function is to transform parameters in the most effective way, so as to enhance the efficiency of the system. Basically, GA will randomly generate N chromosomes and imitate the process of biological evolution, including selection, crossover, and mutations based on good individuals surviving and breed good individuals to optimize the variables problem [115]. An example of the genetic algorithm steps is shown in Figure 8.

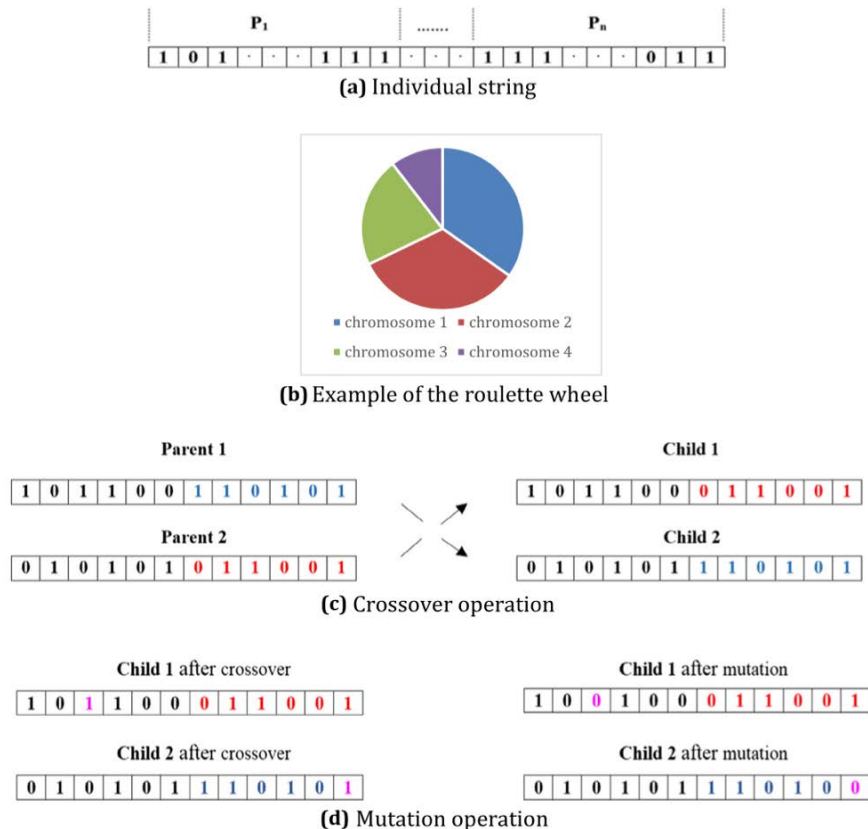


Figure 8. An example of the genetic algorithm steps [115].

Xu et al. [116] used GA to optimize lithium-ion battery model parameters. Zheng Chen et al. [117] proposed GA to estimate the battery model parameters by using battery current and voltage measurements. Besides, the GA-based BP neural network approach proposed by Zuchang Gao [118] shows that it can display a lower error range and higher value.

(5) Fuzzy logic (FL)

Fuzzy logic (FL) is another useful algorithm used to present a non-linear complex model with the help of the appropriate training dataset. Adaptive neuro-fuzzy inference system (ANFIS) methods are proposed to estimate lithium-ion batteries SOC, which are studied in [119–122]. Haifeng Dai et al. [123] proposed a novel approach for online pack SOC estimation, which combines a traditional SOC estimator and an ANFIS. This method has excellent adaptation to different current conditions and the variations of the battery's state, even with an aging process. Figure 9 graphically illustrates a basic ANFIS structure with five layers.

Though fuzzy logic has a powerful ability to predict non-linear models, it requires complex computations and large storage memory units, as well as an expensive processing unit.

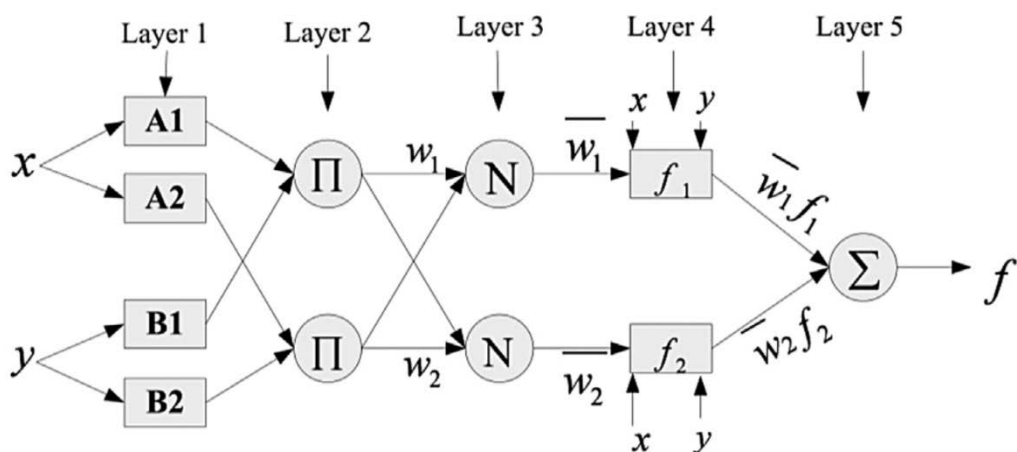


Figure 9. Basic architecture of ANFIS [123].

3.4. Non-Linear Observer

Non-linear observers (NLO), sliding mode observer (SMO), and proportional-integral observer (PIO) theories are proposed to estimate the SOC of lithium-ion batteries [58–63,124,125].

(1) Non-linear Observers (NLO)

Linear and non-linear observers have been used to estimate the system states. Linear observers are commonly used, but will increase the SOC estimation error. Hence, the non-linear observer is used in a linear system with non-linear observation mathematical equations [124]. Chaoren et al. [126] proposed the SOC estimation method based on NLO. Ma et al. [127] proposed a novel state observer based on input-to-state stability (ISS) theory for lithium-ion battery SOC estimation. The results show that the proposed method has a high SOC estimation accuracy with an error of about 2%.

(2) Proportional-integral Observer (PIO)

PIO has been widely applied to the replacement of feedback control system [125]. The function of a PIO controller is to converge the estimated voltage to the measured voltage in an accurate and fast way. Jun Xu [128] proposed the PIO to estimate the SOC of lithium-ion batteries in EVs. The results show that the error is limited to 2% compared with both unknown and known SOC cases by the UDDS driving cycle. An example of the PIO algorithm for SOC estimation is shown in Figure 10.

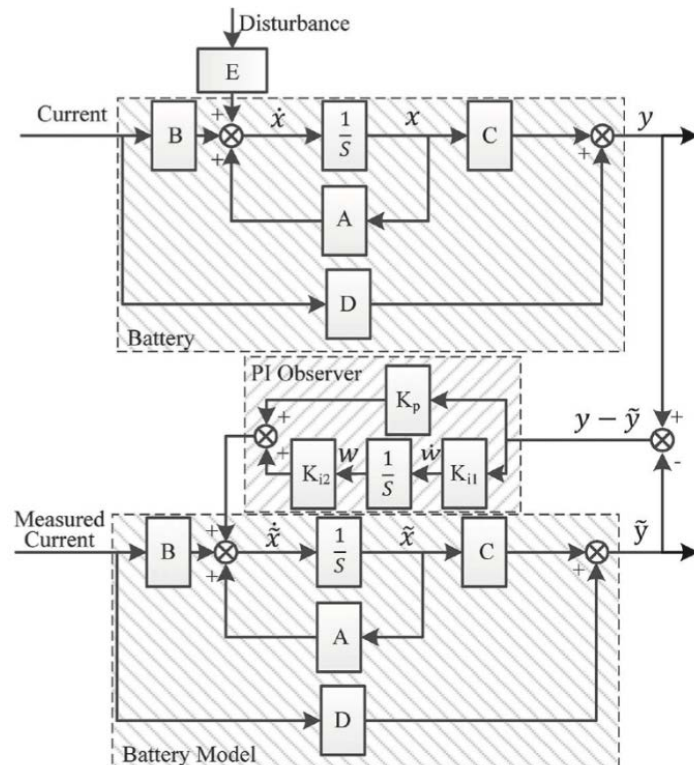


Figure 10. An example of the PIO algorithm for SOC estimation [128].

The PI method has a simple structure and is easy to implement. Hence, this method has a high efficiency and high precision.

(3) Sliding Mode Observer (SMO)

SMO can guarantee the stability and robustness of the system against model uncertainties and environmental disturbances [58–63]. The model is established by using the state equation as the output state and a feedback switching gain is designed to control the sliding regime to ensure the robustness of tracking control.

Kim et al. [129] developed a battery SOC estimation based on the SMO method to compensate for the non-linear dynamic characteristics of the battery for hybrid electric vehicles. The proposed method was able to control the convergence time at a high value of charge or discharge value. UDDS is used to evaluate the performance of the methods and the results show that SOC error is less than 3%. Rui Feng and Wenhui et al. [130] proposed a novel sliding mode observer for SOC estimation. Federal urban driving schedule (FUDS), the West Virginia suburban driving schedule (WVUSUB), and The New European driving cycle (NEDC) experiments are used to validate the performance of the proposed method. Experimental results show that the SOC estimation error is less than 3%.

Compared with results of the EKF method, the SMO method has a faster convergence rate and higher estimation accuracy than the EKF method, but lower computational costs.

3.5. Others and Hybrid Algorithm Method

The hybrid algorithm method is composed of two more algorithms. It can improve the efficiency and accuracy of the battery model and avoid the shortcomings of a single algorithm. The hybrid algorithm method not only achieves reliable and effective results, but also reduces the cost of the battery management system. However, this method has a very complex mathematical calculation, which requires a large storage memory and computing power unit.

(1) EKF-Ah algorithm

Choosing a suitable algorithm is a very important step in estimating SOC. However, in order to improve the accuracy of SOC estimation, the dependence on hardware and cost implications should also be considered. The EKF-Ah optimal estimation algorithm adopted by Qianqian et al. [131] is shown in Table 10, which relies on the current integration method to optimize the estimation with the observation value. Compared with the current integration method, the EKF-Ah algorithm overcomes the interference of the initial value on SOC estimation.

Table 10. Summary of the EKF-Ah algorithm for SOC estimation [131].

State-space model	$x_k = f(x_{k-1}, u_{k-1}) + w_{k-1}$
	$y_k = g(x_k, u_k) + v_k$
Initialization	
For $k = 0$, set	$\hat{x}_0^+ = \mathbb{E}[x_0]$
	$P_{\hat{x},0}^+ = \mathbb{E}[(x_0 - \hat{x}_0^+)(x_0 - \hat{x}_0^+)^T]$
Computation	
For $k = 1, 2, \dots$ compute	
State estimate time update :	$\hat{x}_k^- = A_{k-1}\hat{x}_{k-1}^+ + B_{k-1}u_{k-1}$
Error covariance time update :	$P_{\hat{x},k}^- = A_{k-1}P_{\hat{x},k}^+A_{k-1}^T + \Gamma_{k,k-1}\hat{Q}_{k-1}\Gamma_{k,k-1}^T$
Kalman gain matrix :	$K_k = P_{\hat{x},k}^-\hat{C}_k^T[\hat{C}_kP_{\hat{x},k}^-\hat{C}_k^T + R_{k-1}]^{-1}$
State estimate measurement update:	$\hat{x}_k^+ = \hat{x}_k^- + K_k[y_k - g(\hat{x}_k^+, u_k)]$
Error covariance measurement update:	$P_{\hat{x},k}^+ = (I - K_kC_k)P_{\hat{x},k}^-$

(2) Adaptive Unscented Kalman Filter and Support Vector Machine

Jinhao et al. [132] proposed a highly accurate algorithm for lithium polymer battery SOC estimation based on adaptive unscented Kalman filters (AUKF) and least square support vector machines (LSSVM). A summary of AUKF-LSSVM for SOC estimation is shown in Table 11.

This chapter summarizes the estimation of SOC including coulomb counting, the OCV method, Impedance and internal resistance method, Kalman family and filter method, learning algorithm method, non-linear observer method, hybrid algorithm method, and others [133–135]. In addition to the above estimation methods, there are still other methods in the study, such as a mixture of the Kalman and H_∞ filters method, mixture of SMO and the adaptive Luenberger method, the RBF-PF algorithm, and so on. To verify the advantages and disadvantages of an estimation algorithm, one of the key factors is to test the error of the result. The summary of SOC estimation error is shown in Table 12. There are many reasons for estimated result error in the actual use, such as work environment, hardware, software code technology, battery dynamic hysteresis characteristics, self-discharge, battery aging process, temperature impact, C rate, and cell imbalance, which may lead to a decline in battery performance, so it is not enough to judge the advantages and disadvantages of the algorithm by error alone.

Table 11. Summary of AUKF-LSSVM for SOC estimation [131].

State-space and LSSVMmodel	
	$X_k = f(X_k, i_k) + q_k = X_k - \frac{\eta}{Q_n} \cdot \Delta t \cdot i_k + q_k$
	$Z_{k+1} = H(X_k, i_k) + r_k$
	$H(X_k, i_k) = \sum_{i=1}^l a_i K(x_j, i_j) + b$
Initialization	
For $k = 0$, set	
	$\hat{x}_0^+ = \mathbb{E}[x_0]$
	$P_{\hat{x},0}^+ = \mathbb{E}[(x_0 - \hat{x}_0^+)(x_0 - \hat{x}_0^+)^T]$
Computation	
Generate sigma points and weighting coefficients at time $k - 1$, ($k \in [1, \dots, \infty]$)	
	$\tilde{x}_0 = \hat{x}_{k-1}$
	$\tilde{x}_{k-1}^{(i)} = \hat{x}_{k-1} + (\sqrt{(n + \lambda) P_{k-1}})_i$
	$\tilde{x}_{k-1}^{(j)} = \hat{x}_{k-1} - (\sqrt{(n + \lambda) P_{k-1}})_{j-n}$
	$W_m^{(0)} = \lambda / (n + \lambda)$
	$W_c^{(0)} = \lambda / (n + \lambda) + 1 - \alpha^2 + \beta$
	$W_m^{(i)} = W_c^{(i)} = \lambda / [2(n + \lambda)]$
Prediction and correction:	
For $k = 1, 2, \dots$ compute	
State estimate time update:	
	$\tilde{x}_{k k-1}^{(i)} = f(\tilde{x}_{k k-1}^{(i)}, i_k)$
	$\hat{x}_{k-1} = \sum_{i=0}^{2n} W_m^{(i)} \cdot \tilde{x}_{k k-1}^{(i)}$
	$P_{x,k k-1}^- = \sum_{i=0}^{2n} W_c^{(i)} [\tilde{x}_{k k-1}^{(i)} - \hat{x}_{k-1}] [\tilde{x}_{k k-1}^{(i)} - \hat{x}_{k-1}]^T + q_{k-1}$
	$Z_{k k-1}^{(i)} = H(\hat{x}_{k k-1}^{(i)}, i_k)$
	$\hat{Z}_{k-1} = \sum_{i=0}^{2n} W_m^{(i)} \cdot Z_{k k-1}^{(i)}$
Correction update	
	$P_{y,k} = \sum_{i=0}^{2n} W_c^{(i)} [Z_{k k-1}^{(i)} - \hat{Z}_{k-1}] [Z_{k k-1}^{(i)} - \hat{Z}_{k-1}]^T + r_{k-1}$
	$P_{xy,k} = \sum_{i=0}^{2n} W_c^{(i)} [X_{k k-1}^{(i)} - \hat{X}_{k-1}] [X_{k k-1}^{(i)} - \hat{X}_{k-1}]^T$
	$K_k = P_{xy,k} P_{y,k}^{-1}$
	$\hat{x}_k = \hat{x}_{k k-1} + K_k (Z_k - \hat{Z}_{k k-1})$
	$P_k = P_{x,k k-1}^- - K_k P_{y,k} K_k^T$
Adjustment process:	
	$\varepsilon_k = Z_k - H(\hat{x}_k, i_k)$
	$c_k = \frac{\sum_{i=k-L+1}^k \varepsilon_k \varepsilon_k^T}{L}$
	$r_k = c_k + \sum_{i=0}^{2n+1} W_c^{(i)} [Z_{k k-1}^{(i)} - Z_k + c_k] [Z_{k k-1}^{(i)} - Z_k + c_k]^T$
	$q_k = K_k c_k K_k^T$

Table 12. Maximum absolute error of different SOC methods.

Method	Model	Conditions	Battery	MAE	Author	Ref
EMF	-	-	NMC	$\leq 2\%$	Wladislaw Waag et al.	[85]
KF	1RC	CC	Li-ion battery	$\leq 1.76\%$	Yatsui and Bai	[87]
DEKF			Li-ion battery		Lee et al.	[96]
FKF	1RC	UDDS Real driving cycle	LiFePO4	$\leq 2\%$ $\leq 3\%$	KaiChin Lim et al.	[53]
EKF	2RC	UDDS and HWFET	Li-ion battery	$\leq 3\%$	Chen et al.	[97]
AEKF	1RC	UDDS	Li-ion battery	$\leq 2\%$	Xiong et al.	[100]
UKF	Rint	FUDS	LiFePO4	$\leq 2.16\%$	Yinjiao Xing et al.	[102]
SPKF	ESC	UDDS	LiPB	$\leq 0.49\%$	Gregory L. Plett et al.	[103]
DPF DAPF	Thevenin model	UDDS	NMC	$\leq 2.27\%$ $\leq 1.33\%$ (MSE)	Min Ye et al.	[107]
AHF	-	-	Li-ion battery	$\leq 0.84\%$	Mohammad Charkhgard et al.	[108]
PSO-SVR ANN	-	Real driving cycle	LiFePO4	$\leq 0.17\%$ $\leq 0.25\%$	Hanmin Sheng et al.	[114]
Fuzzy-LSSVM	-	Real driving cycle	LiFePO4	$\leq 0.5\%$	Hanmin Sheng et al.	[114]
GA	1RC	UDDS	Li-ion battery	$\leq 1\%$	Jun Xu et al.	[116]
ANFIS	-	FTP75/J1015/EUDC	Li-ion battery	More reasonable	Haifeng Dai et al.	[123]
NLO	2RC	-	Li-ion battery	$\leq 2\%$	Ma et al.	[127]
PIO	1RC	UDDS	Li-ion battery	$\leq 2\%$	Jun Xu et al.	[128]
SMO	2RC	FUDS/NEDC/WVUSUB	NMC	$\leq 3\%$	Ruifeng et al.	[130]

4. SOC Issues and Challenges

The accuracy of SOC estimation in a battery system is necessary and important. For the battery cell, an accurate SOC can provide precise parameters to make a better lithium-ion battery cell. For the EV battery systems, an accurate SOC can prevent the battery from over-discharge and charge, thus ensuring battery system safety, making more efficient use of the limited energy, and extending the battery life. Specifically, it can support the precise calculation of the vehicle driving range, provide a better discharging or charging strategy, improve the efficiency of other power sources, and make balance strategies work more effectively. The lithium-ion battery SOC estimation in EVs has become a major challenge due to its complex electrochemical reactions and performance degradation caused by various factors [4].

In order to improve the accuracy, stability, robustness, economy, and other challenges of the SOC estimation algorithm in electric vehicles, these issues, such as lithium-ion battery hysteresis characteristic, battery model, aging, estimation algorithm, and cell unbalancing, are worth studying in depth and are also solutions to solve SOC estimation problems.

4.1. Lithium-Ion Battery Hysteresis Characteristic

Due to the lithium-ion battery having a polarization phenomenon, this phenomenon will lead to the battery dynamic hysteresis characteristics. Because of battery dynamic hysteresis characteristics, the OCV curve of the charging and discharging process is different, as shown in Figure 11. The battery OCV of the charging process is higher than discharging.

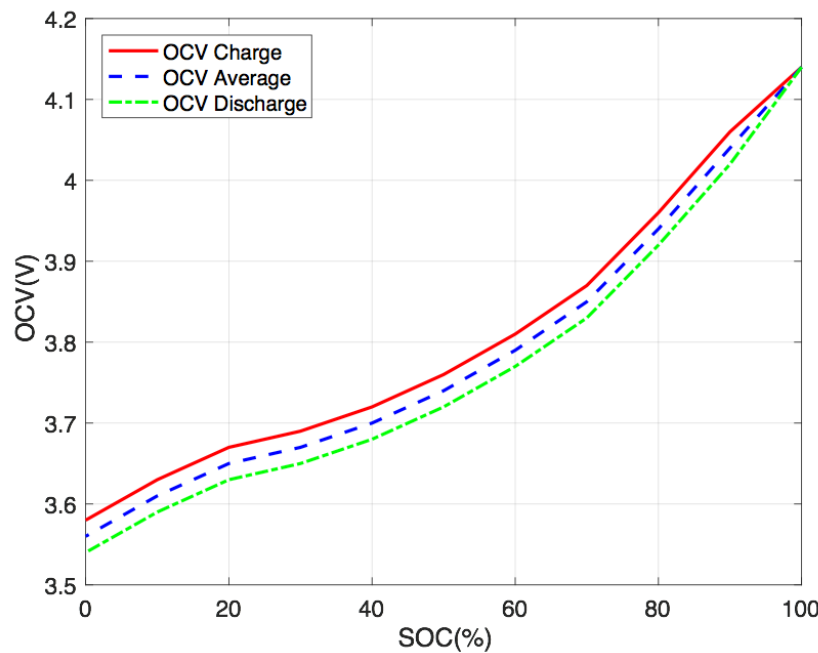


Figure 11. SOC-OCV curves under the charge and discharge process.

Thus, the SOC-OCV curve is not consistent with the charge and discharge. Even for a battery under the same discharge/charge, the SOC-OCV curve performance is very different under different temperature conditions, as shown in Figure 12. Furthermore, the SOC-OCV curve will be drifting when the battery ages. There are also great differences in SOC-OCV under different material systems. For example, the SOC-OCV platform of LiFePO₄ is very flat, which will bring some error to the accurate estimation of SOC. SOC-OCV characteristics under different temperatures and aging at different SOCs are shown in Figure 13.

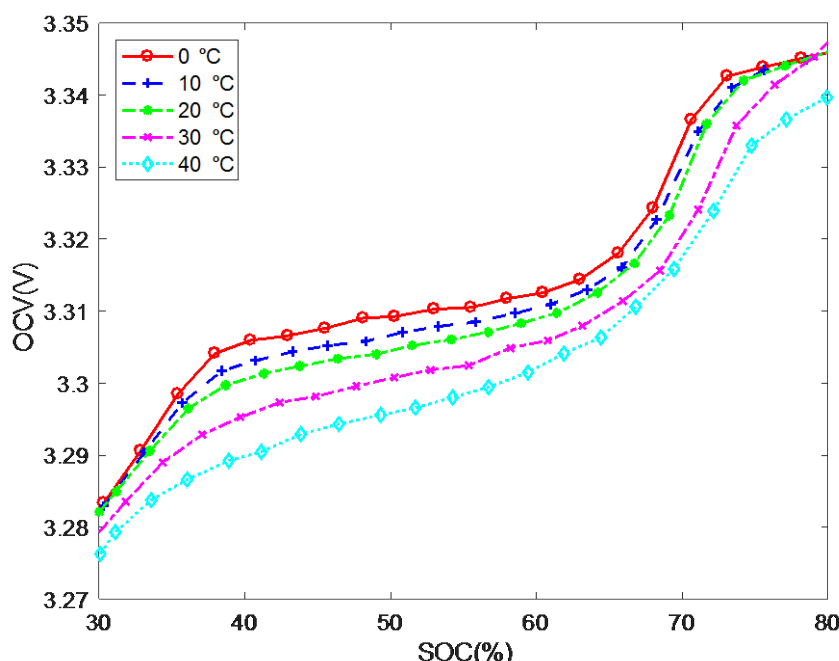


Figure 12. SOC-OCV curves at different temperatures.

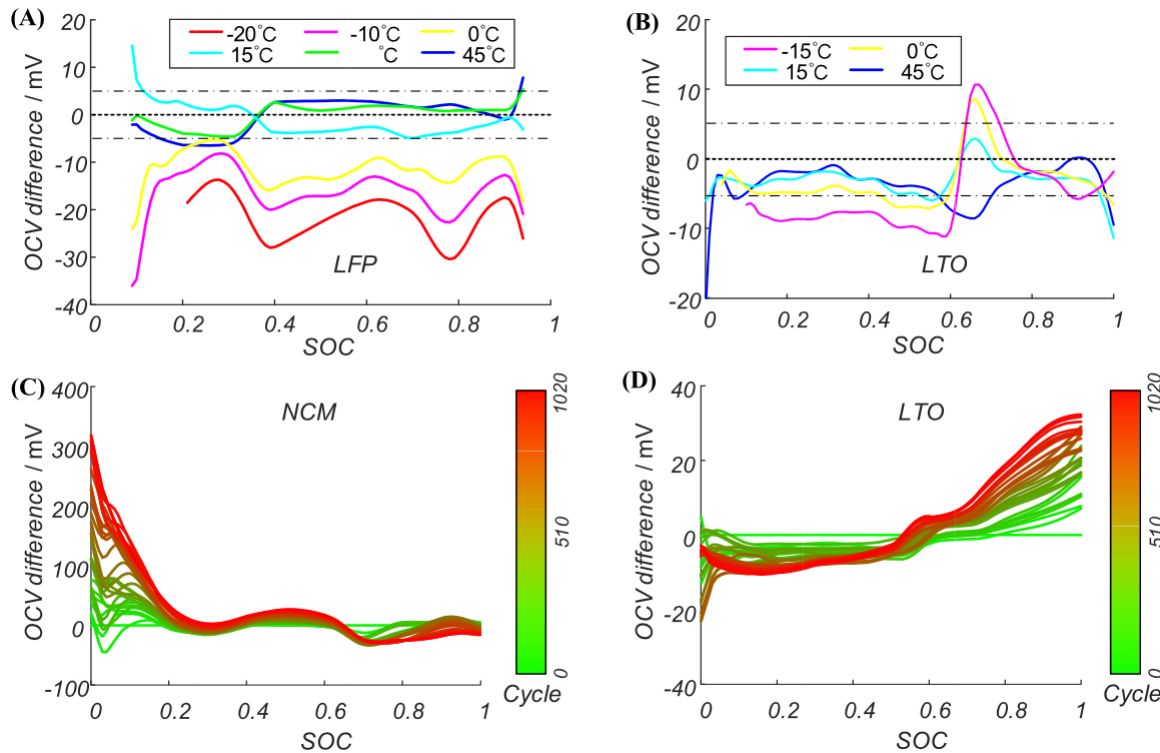


Figure 13. OCV characteristics under different temperatures and ageing at different SOCs. (A) LFP cell; (B) LTO cell; (C) NCM cell; (D) LTO cell [83].

The SOC-OCV curve drifting after two calendar years of ageing is shown in Figure 14. In order to overcome the challenges of aging, Lavigne et al. [136] proposed a two stage lithium-ion OCV curve model to estimate battery SOC.

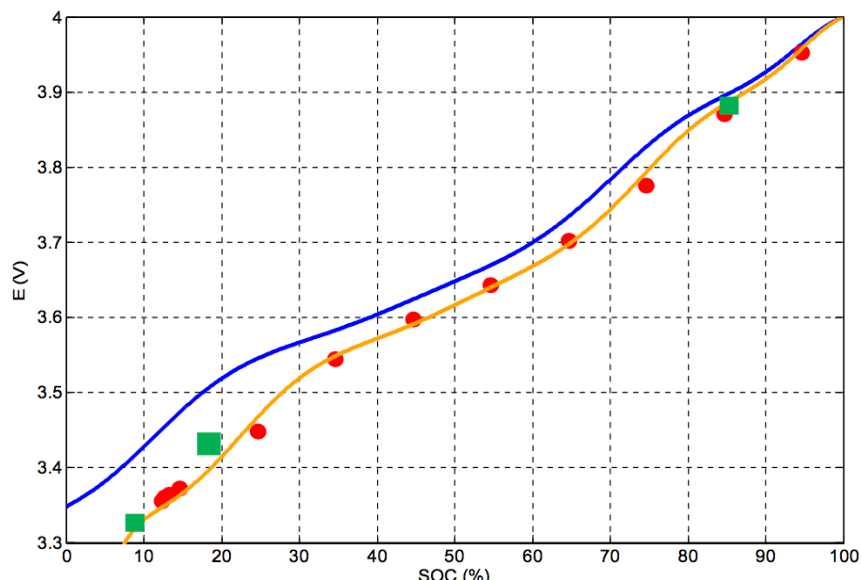


Figure 14. The SOC-OCV curve drifting after two calendar years of ageing. (Blue line is the initial OCV curve; Orange line is the aged OCV curve; Red dots are measured at 3 years; Green box are measured for parameter identification) [136].

4.2. Lithium-Ion Battery Model

The state parameters of positive and negative electrodes, such as electricity, OCV, impedance, internal resistance, and Li amount, are related to the SOC estimation of lithium-ion batteries. In order to realize the identification of these parameters and estimate the battery state, a battery model is needed. A lithium-ion battery model can be classified as an electrochemical model, physical model, equivalent circuit model (ECMs), thermal model, coupled electro-thermal model, and so on. Among them, ECMs are the most commonly used in lithium-ion batteries SOC estimation for EV applications due to their simple model structure.

ECMs such as the Rint model, Thevenin model, PNGV model, GNL, n RC model, and FOM (Fractional Order Model), are shown in Figure 15. The Rint model is very simple to implement in real time. However, the model's output equation expressed is only a rough estimate actual terminal voltage of the battery, which may lead to large uncertainties in SOC estimates [30]. The Thevenin model connects a parallel RC network in series based on the Rint model [31]. The PNGV model can be used to describe the changing of open circuit voltage generated in the time accumulation of load current by adding a capacitor in series based on the Thevenin model [31]. The GNL nonlinear equivalent circuit battery model takes into account the influence of the self-discharge on characteristics of the battery [137]. The nRC consists of an n parallel RC network in series based on the Thevenin model in order to considering dynamic voltage performances [138]. In order to conquer the traditional ECMs shortcoming and guarantee the optimal trade-off between model complexity and computation efficiency, the fractional order model impedance model is studied by [37].

These battery ECM models and equations are summarized in Table 13.

Table 13. Battery ECM models and equations.

Model	Equation
Rint	$U_t = U_{oc} - IR_0$
Thevenin	$\begin{cases} \dot{U}_1 = \frac{I}{C_1} - \frac{U_1}{R_1 C_1} \\ U_t = U_{OC} - U_1 - IR_0 \end{cases}$
PNGV	$\begin{cases} \dot{U}_b = U'_{oc} \\ \dot{U}_1 = \frac{I}{C_1} - \frac{U_1}{R_1 C_1} \\ U_t = U_{OC} - U_b - U_1 - IR_0 \end{cases}$
GNL	$\begin{cases} \dot{U}_b = U'_{oc} \\ \dot{U}_1 = \frac{I}{C_1} - \frac{U_b}{C_1 R_s} - \left(\frac{U_1}{C_1 R_s} + \frac{U_1}{C_1 R_1} \right) - \frac{U_2}{C_1 R_s} - \frac{U_{oc}}{C_1 R_s} \\ \dot{U}_2 = \frac{I}{C_2} - \frac{U_b}{C_2 R_s} - \left(\frac{U_2}{C_2 R_s} + \frac{U_2}{C_2 R_2} \right) - \frac{U_1}{C_2 R_s} - \frac{U_{oc}}{C_2 R_s} \\ U_t = U_{OC} - U_b - U_1 - U_2 - IR_0 \end{cases}$
n RC	$\begin{cases} \dot{U}_{Di} = -\frac{1}{R_{Di} C_{Di}} U_{Di} + \frac{1}{C_{Di}} I_L \\ U_t = U_{oc} - \sum_{i=1}^n U_{Di} - I_L R_0 \end{cases}$
FOM	$\begin{cases} D^{n_1} \dot{U}_1 = \frac{I}{C_1} - \frac{U_1}{C_1 R_1} \\ D^{n_2} \dot{U}_2 = \frac{I}{C_2} - \frac{U_2}{C_2 R_2} \\ U_t = U_{OC} - U_1 - U_2 - IR_0 \end{cases}$

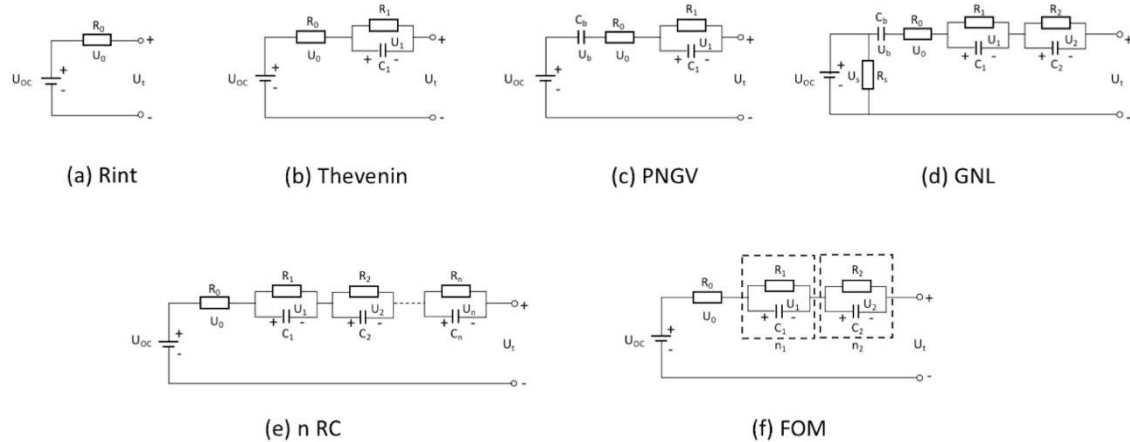


Figure 15. The commonly used battery electrical equivalent circuit model.

Different battery anode-cathode material systems have different properties. Therefore, different battery models are needed to simulate different types of batteries. Battery modeling has an important influence on SOC estimation. Establishing a battery model is a challenge, because of the complex electrochemical and dynamic environment. Each model may lack accuracy and adaptability to use in different operating conditions. In addition, the battery hysteresis effect is not considered in many ECMS. So, we need to develop a suitable battery model that can work accurately under different load conditions.

4.3. Lithium-Ion Battery Aging

Due to battery aging, SOC could not be accurately estimated. Degradation of internal resistance and capacitance, and available power fade are the main factors leading to battery aging. Main aging causes for Li-ion batteries are the decomposition of solid electrolyte interphase (SEI), deposition at the anode, metal dissolution from the anode, the loss of active material, and lithium plating [139]. The analysis of the reasons for battery aging is shown in Figure 16.

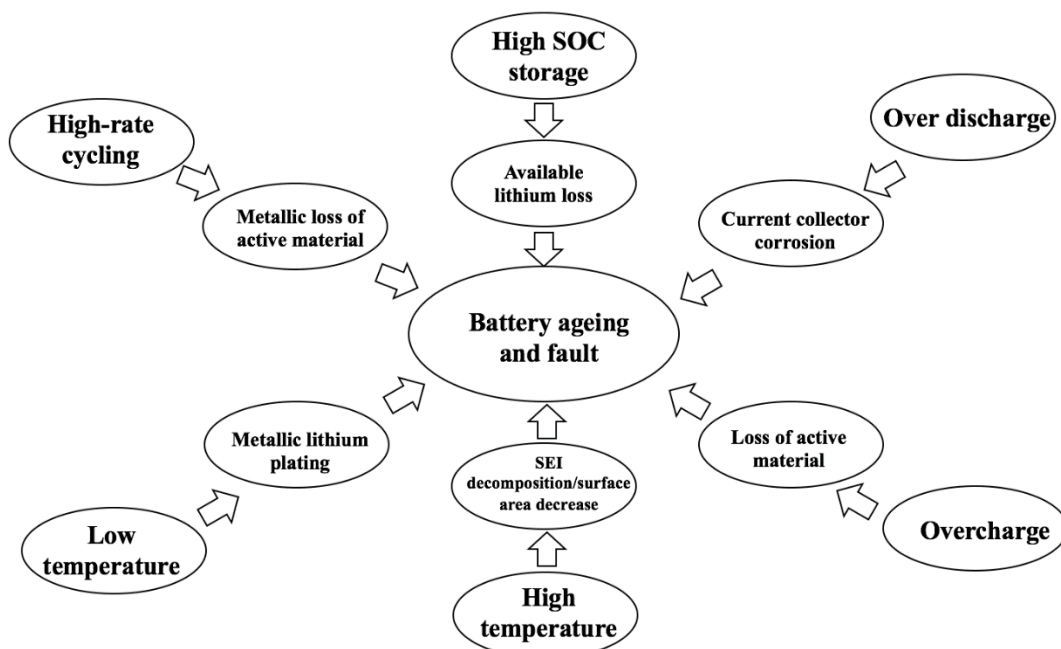


Figure 16. Analysis of the reasons for battery aging [139].

4.4. Estimation Algorithm

Figure 17 approximately demonstrates the estimation error and computational complexity of the SOC estimation methods, according to the estimation algorithm study. Compared to the six SOC estimation families, the Ah counting estimation method, based on the OCV estimation method and based on the ECM model, and the filter algorithms estimation method are the main three SOC estimation families, which are currently applicable EVs for online applications [83].

At present, the most potential and most widely used SOC estimation algorithm in the battery management system of electric vehicles is a hybrid algorithm based on the combination of the equivalent circuit model and the Kalman filter algorithm family. The most significant error source of this method is that the voltage and current sensor drifts the battery model shortcoming, for which the influence of the variable effect are not enough, for example, the aging, temperature, and hysteresis effect. Thus, we should focus on these error factors, and solve the sensor drift, aging, temperature, and hysteresis effect problems.

Other measurements, such as the ultrasound velocity [140], magnetic field intensity [141], or mechanical stress [142] can also be used for some special SOC estimation in research. Nevertheless, the feasibility is poor because additional sensors are needed. Besides, the accuracy is also questionable.

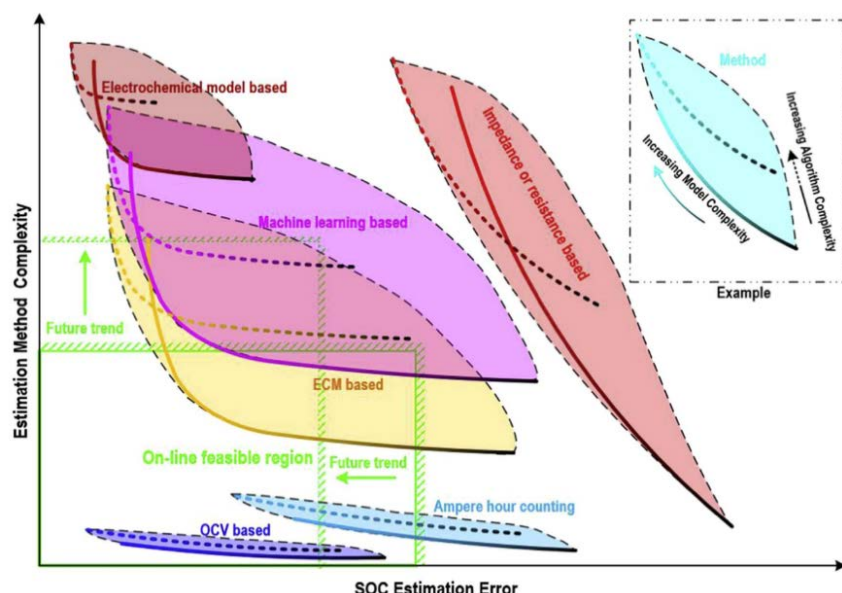


Figure 17. Estimation error and computational complexity for the commonly studied SOC estimation methods [83].

4.5. Cell Unbalancing

In the application of electric vehicles, the battery system is made up of numerous single cells in series and parallel. Because of the difference in the complex chemical composition, manufacturing process, environment temperature, and operating conditions of each cell, cell imbalance can be caused by the use process. Using the same estimation algorithm to estimate the SOC value of all battery cell or module will also bring greater error to the overall SOC estimation accuracy of the electric vehicle. The control strategy and the management mode of the battery system are affected. Therefore, in addition to improving the estimation accuracy of the battery cell, it is necessary to effectively monitor the state of each cell and precise control cell balance to improve the overall estimation accuracy of the SOC of the electric vehicle so that electric vehicle battery pack can deliver energy for long periods and safety [4]. In order to simulate the battery pack model efficiently, Zuchang Gao et al. [143] proposed

prototyping a simulation model to determine the SOC and temperature of the battery working in a real world environment.

5. Conclusions

The paper describes the evolution of battery SOC estimation and various SOC estimation family algorithms were reviewed. The development and deployment of an EVs battery management system with the state estimation of SOC has been a major challenge as a result of the complex electrochemical reactions and performance degradation caused by a variety of factors. Battery dynamic hysteresis characteristics, self-discharge, ambient temperature, battery aging, C rate, and cell unbalancing are the other reasons responsible for the accuracy of SOC estimation. SOC estimation based on ECMs with the KF family method should pay more attention to the sensor drift and battery OCV hysteresis effect instead of using a more complicated algorithm according to this paper study.

Because of the severe demand of electric vehicles, the variety of battery developments will become more and more, and the electrochemical components and performance of all kinds of batteries are different, which will bring a lot of uncertainty and challenges to the general SOC estimation. In order to improve the research and application of electric vehicle battery estimation, two kinds of basic accumulation are essential. On one hand, it is needed to establish a full-type and full-life cycle test database, but this method will occupy a lot of time and cost; on the other hand, it is used to establish a foundation based battery simulation and verification tool, including the simulation software tool from the battery cell simulation, the battery model module simulation, the battery estimation simulation, to the battery heat management simulation, in order to accelerate the battery from the cell prototype design to the pack practical application. Although the battery simulation and verification base tool will include a high cost and long time, it is very meaningful and worthy of our research in the future.

Author Contributions: R.Z. studied scientific and technical literature, and wrote the review paper; B.X., Y.L., W.Z., H.W., and W.W. provided materials and equipment; B.L. and L.C. gave paper guidance.

Funding: This work was supported by the Shenzhen Economic, Trade and Information Commission “Innovation Chain + Industrial Chain” Project (2017), China Postdoctoral Science Foundation (Grant No. 2017M622799), and The State Key Laboratory of Advanced Design and Manufacturing for Vehicle Body Open Fund (Grant No. 31715013).

Acknowledgments: The authors would like to thank the Shenzhen Economic, Trade and Information Commission, China Postdoctoral Science, The State Key Laboratory of Advanced Design and Manufacturing for Vehicle Body Open Fund, and Tan, for their technical support.

Conflicts of Interest: The authors declare that there is no conflict of interest.

Nomenclature

Acronyms

A	Ampere
Ah	Ampere-hour
AI	Artificial Intelligence
EV	Electrical Vehicle
BMS	Battery Management System
BTMS	Battery Thermal Management System
CC	Constant Current
CCCV	Constant Current-Constant Voltage
CKF	Cubature Kalman Filter
CV	Constant Voltage
EIS	Electrochemical Impedance Spectroscopy
EKF	Extend Kalman filter
EMC	Equivalent Circuit Model
EUDC	Extra Urban Driving Cycle
EV	Electric Vehicle
HPPC	The Hybrid Power Pulse Characteristics

KF	Kalman Filter
LCO	Lithium cobalt oxide
LMO	Lithium Manganese Oxide
LFP	Lithium Iron Phosphate
LTO	Lithium Titanium Oxide
NEDC	New European Driving Cycle
NCA	Nickel Cobalt Aluminum
NMC	Nickel Manganese Cobalt
OCV	Open-Circuit Voltage
MRSTEKF	Multirate Strong Tracking Extended Kalman Filter
PF	Particle Filter
P2D	Pseudo-two-Dimensional
SMO	Sliding Mode Observer
SOC	State of Charge
SOE	State of Energy
SOH	State of Health
SOP	State of Power
SPKF	Sigma-point Kalman Filter
STCEKF	Strong Tracking Cubature Extended Kalman Filter
SVM	Support Vector Machine
UKF	Unscented Kalman Filter
V	Volt

Symbols

α	Fading factor
β	Attenuation factor
σ	Standard deviation of the noise variance
C_n	Nominal capacity of the battery
I	Load current
k	Time step
Q_w, R_v	Gaussian noise processes of covariance matrices
S_d	Self-discharging rate
t	Time
T	Sampling period
x_k	Stated equation
y_k	Output equation
u_k, w_k	System and process noise
η	Coulombic efficiency

Subscript

min	Minimum value
max	Maximum value

Abbreviations

UDDS	Urban Dynamometer Driving Schedule
USABC	U.S. Advanced Battery Consortium
FPGA	Field Programmable Gate Array
RMSE	Root Mean Square Error

References

1. Horie, H. Application study of li-ion battery for EVs and HEVs. *J. Surf. Finish. Soc. Jpn.* **1997**, *48*, 1148–1152. [[CrossRef](#)]
2. Batteries, A.A.L. Aprotic and aqueous Li-O₂ batteries. *Chem. Rev.* **2014**, *114*, 5611–5640.
3. Burke, A.F. Batteries and ultracapacitors for electric, hybrid, and fuel cell vehicles. *Proc. IEEE* **2007**, *95*, 806–820. [[CrossRef](#)]

4. Hannan, M.A.; Lipu, M.S.H.; Hussain, A.; Mohamed, A. A review of lithium-ion battery state of charge estimation and management system in electric vehicle applications: Challenges and recommendations. *Renew. Sustain. Energy Rev.* **2017**, *78*, 834–854. [[CrossRef](#)]
5. Goodenough, J.B.; Kim, Y. Challenges for rechargeable Li batteries. *Chem. Mater.* **2014**, *22*, 587–603. [[CrossRef](#)]
6. Ianniciello, L.; Biwolé, P.H.; Achard, P. Electric vehicles batteries thermal management systems employing phase change materials. *J. Power Sources* **2018**, *378*, 383–403. [[CrossRef](#)]
7. Girishkumar, G.; McCloskey, B.; Luntz, A.C.; Swanson, S.; Wilcke, W. Lithium–air battery: Promise and challenges. *J. Phys. Chem. Lett.* **2010**, *1*, 2193–2203. [[CrossRef](#)]
8. Sun, Z.; Wang, S.; Yan, L.; Xiao, M.; Han, D.; Meng, Y. Mesoporous carbon materials prepared from litchi shell as sulfur encapsulator for lithium-sulfur battery application. *J. Power Sources* **2016**, *324*, 547–555. [[CrossRef](#)]
9. Propp, K.; Auger, D.J.; Fotouhi, A.; Longo, S.; Knap, V. Kalman-variant estimators for state of charge in lithium-sulfur batteries. *J. Power Sources* **2017**, *343*, 254–267. [[CrossRef](#)]
10. Urbonaitė, S.; Novák, P. Importance of ‘unimportant’ experimental parameters in Li–S battery development. *J. Power Sources* **2014**, *249*, 497–502. [[CrossRef](#)]
11. Huff, L.A.; Rapp, J.L.; Baughman, J.A.; Rinaldi, P.L.; Gewirth, A.A. Identification of lithium–sulfur battery discharge products through ^{6}Li and ^{33}S solid-state MAS and ^{7}Li solution NMR spectroscopy. *Surf. Sci.* **2015**, *631*, 295–300. [[CrossRef](#)]
12. Shen, X.; Liu, H.; Cheng, X.-B.; Yan, C.; Huang, J.-Q. Beyond lithium ion batteries: Higher energy density battery systems based on lithium metal anodes. *Energy Storage Mater.* **2018**, *12*, 161–175. [[CrossRef](#)]
13. Sun, L.; Li, H.; Zhao, M.; Wang, G. High-performance lithium-sulfur batteries based on self-supporting graphene/carbon nanotube foam@sulfur composite cathode and quasi-solid-state polymer electrolyte. *Chem. Eng. J.* **2018**, *332*, 8–15. [[CrossRef](#)]
14. Liu, X.; Huang, J.-Q.; Zhang, Q.; Mai, L. Nanostructured metal oxides and sulfides for lithium–sulfur batteries. *Adv. Mater.* **2017**, *29*, 1601759. [[CrossRef](#)] [[PubMed](#)]
15. Gao, P.; Zhang, C.; Wen, G. Equivalent circuit model analysis on electrochemical impedance spectroscopy of lithium metal batteries. *J. Power Sources* **2015**, *294*, 67–74. [[CrossRef](#)]
16. Xu, W.; Wang, J.; Ding, F.; Chen, X.; Nasybulin, E.; Zhang, Y.; Zhang, J.G. Lithium metal anodes for rechargeable batteries. *Energy Environ. Sci.* **2014**, *7*, 513–537. [[CrossRef](#)]
17. Sun, C.; Liu, J.; Gong, Y.; Wilkinson, D.P.; Zhang, J. Recent advances in all-solid-state rechargeable lithium batteries. *Nano Energy* **2017**, *33*, 363–386. [[CrossRef](#)]
18. Wang, P.; Chen, H.; Li, N.; Zhang, X.; Jiao, S.; Song, W.-L.; Fang, D. Dense graphene papers: Toward stable and recoverable Al-ion battery cathodes with high volumetric and areal energy and power density. *Energy Storage Mater.* **2018**, *13*, 103–111. [[CrossRef](#)]
19. Mebarki, N.; Rekioua, T.; Mokrani, Z.; Rekioua, D.; Bacha, S. PEM fuel cell/ battery storage system supplying electric vehicle. *Int. J. Hydrogen Energy* **2016**, *41*, 20993–21005. [[CrossRef](#)]
20. Rurgladdapan, J.; Uthaichana, K.; Kaewkham-ai, B. Optimal Li-Ion battery sizing on PEMFC hybrid powertrain using dynamic programming. In Proceedings of the 2013 8th IEEE Conference on Industrial Electronics and Applications (ICIEA), Melbourne, VIC, Australia, 19–21 June 2013; pp. 472–477.
21. Caisheng, W.; Nehrir, M.H. Fuel cells and load transients. *IEEE Power Energy Mag.* **2007**, *5*, 58–63.
22. Andreasen, S.J.; Ashworth, L.; Menjón Remón, I.N.; Kær, S.K. Directly connected series coupled HTPEM fuel cell stacks to a Li-ion battery DC bus for a fuel cell electrical vehicle. *Int. J. Hydrogen Energy* **2008**, *33*, 7137–7145. [[CrossRef](#)]
23. Zequine, C.; Ranaweera, C.K.; Wang, Z.; Dvornic, P.R.; Kahol, P.K.; Singh, S.; Tripathi, P.; Srivastava, O.N.; Singh, S.; Gupta, B.K. High-performance flexible supercapacitors obtained via recycled jute: Bio-waste to energy storage approach. *Sci. Rep.* **2017**, *7*, 1174. [[CrossRef](#)] [[PubMed](#)]
24. Repp, S.; Harputlu, E.; Gurgen, S.; Castellano, M.; Kremer, N.; Pompe, N.; Wörner, J.; Hoffmann, A.; Thomann, R.; Emen, F.M. Synergetic effects of Fe^{3+} doped spinel $\text{Li}_4\text{Ti}_5\text{O}_{12}$ nanoparticles on reduced graphene oxide for high surface electrode hybrid supercapacitors. *Nanoscale* **2017**, *7*, 11222. [[CrossRef](#)] [[PubMed](#)]
25. Fleischer, C.; Waag, W.; Heyn, H.-M.; Sauer, D.U. On-line adaptive battery impedance parameter and state estimation considering physical principles in reduced order equivalent circuit battery models: Part 1. Requirements, critical review of methods and modeling. *J. Power Sources* **2014**, *260*, 276–291. [[CrossRef](#)]

26. He, H.; Xiong, R.; Guo, H.; Li, S. Comparison study on the battery models used for the energy management of batteries in electric vehicles. *Energy Convers. Manag.* **2012**, *64*, 113–121. [[CrossRef](#)]
27. Schmidt, A.P.; Bitzer, M.; Imre, Á.W.; Guzzella, L. Lumped Parameter Modeling of Electrochemical and Thermal Dynamics in Lithium-Ion Batteries. *IFAC Proc. Vol.* **2010**, *43*, 198–203. [[CrossRef](#)]
28. Oh, K.-Y.; Samad, N.A.; Kim, Y.; Siegel, J.B.; Stefanopoulou, A.G.; Epureanu, B.I. A novel phenomenological multi-physics model of Li-ion battery cells. *J. Power Sources* **2016**, *326*, 447–458. [[CrossRef](#)]
29. Fotouhi, A.; Auger, D.J.; Propp, K.; Longo, S.; Wild, M. A review on electric vehicle battery modelling: From Lithium-ion toward Lithium–Sulphur. *Renew. Sustain. Energy Rev.* **2016**, *56*, 1008–1021. [[CrossRef](#)]
30. Nejad, S.; Gladwin, D.T.; Stone, D.A. A systematic review of lumped-parameter equivalent circuit models for real-time estimation of lithium-ion battery states. *J. Power Sources* **2016**, *316*, 183–196. [[CrossRef](#)]
31. He, H.; Xiong, R.; Fan, J. Evaluation of lithium-ion battery equivalent circuit models for state of charge estimation by an experimental approach. *Energies* **2011**, *4*, 582–598. [[CrossRef](#)]
32. Lin, C. Comparison of current input equivalent circuit models of electrical vehicle battery. *Chin. J. Mech. Eng.* **2005**, *41*, 76–81. [[CrossRef](#)]
33. Liu, C.; Liu, W.; Wang, L.; Hu, G.; Ma, L.; Ren, B. A new method of modeling and state of charge estimation of the battery. *J. Power Sources* **2016**, *320*, 1–12. [[CrossRef](#)]
34. Dong, G.; Wei, J.; Zhang, C.; Chen, Z. Online state of charge estimation and open circuit voltage hysteresis modeling of LiFePO₄ battery using invariant imbedding method. *Appl. Energy* **2016**, *162*, 163–171. [[CrossRef](#)]
35. Feng, T.; Yang, L.; Zhao, X.; Zhang, H.; Qiang, J. Online identification of lithium-ion battery parameters based on an improved equivalent-circuit model and its implementation on battery state-of-power prediction. *J. Power Sources* **2015**, *281*, 192–203. [[CrossRef](#)]
36. Fleischer, C.; Waag, W.; Heyn, H.-M.; Sauer, D.U. On-line adaptive battery impedance parameter and state estimation considering physical principles in reduced order equivalent circuit battery models part 2. Parameter and state estimation. *J. Power Sources* **2014**, *262*, 457–482. [[CrossRef](#)]
37. Mu, H.; Xiong, R.; Zheng, H.; Chang, Y.; Chen, Z. A novel fractional order model based state-of-charge estimation method for lithium-ion battery. *Appl. Energy* **2017**, *207*, 384–393. [[CrossRef](#)]
38. Sabatier, J.; Francisco, J.M.; Guillemard, F.; Lavigne, L.; Moze, M.; Merveillaut, M. Lithium-ion batteries modeling: A simple fractional differentiation based model and its associated parameters estimation method. *Signal Process.* **2015**, *107*, 290–301. [[CrossRef](#)]
39. Sabatier, J.; Aoun, M.; Oustaloup, A.; Grégoire, G.; Ragot, F.; Roy, P. Fractional system identification for lead acid battery state of charge estimation. *Signal Process.* **2006**, *86*, 2645–2657. [[CrossRef](#)]
40. Burgos, C.; Sáez, D.; Orchard, M.E.; Cárdenas, R. Fuzzy modelling for the state-of-charge estimation of lead-acid batteries. *J. Power Sources* **2015**, *274*, 355–366. [[CrossRef](#)]
41. Gandolfo, D.; Brandão, A.; Patiño, D.; Molina, M. Dynamic model of lithium polymer battery—Load resistor method for electric parameters identification. *J. Energy Inst.* **2015**, *88*, 470–479. [[CrossRef](#)]
42. Yang, F.; Wang, D.; Xing, Y.; Tsui, K.-L. Prognostics of Li(NiMnCO)O₂-based lithium-ion batteries using a novel battery degradation model. *Microelectron. Reliab.* **2017**, *70*, 70–78. [[CrossRef](#)]
43. Fridholm, B.; Wik, T.; Nilsson, M. Robust recursive impedance estimation for automotive lithium-ion batteries. *J. Power Sources* **2016**, *304*, 33–41. [[CrossRef](#)]
44. Dai, H.; Xu, T.; Zhu, L.; Wei, X.; Sun, Z. Adaptive model parameter identification for large capacity Li-ion batteries on separated time scales. *Appl. Energy* **2016**, *184*, 119–131. [[CrossRef](#)]
45. Zou, C.; Manzie, C.; Nešić, D.; Kallapur, A.G. Multi-time-scale observer design for state-of-charge and state-of-health of a lithium-ion battery. *J. Power Sources* **2016**, *335*, 121–130. [[CrossRef](#)]
46. Li, Y.; Chattopadhyay, P.; Ray, A.; Rahn, C.D. Identification of the battery state-of-health parameter from input–output pairs of time series data. *J. Power Sources* **2015**, *285*, 235–246. [[CrossRef](#)]
47. Dong, G.; Chen, Z.; Wei, J.; Zhang, C.; Wang, P. An online model-based method for state of energy estimation of lithium-ion batteries using dual filters. *J. Power Sources* **2016**, *301*, 277–286. [[CrossRef](#)]
48. He, H.; Zhang, Y.; Xiong, R.; Wang, C. A novel Gaussian model based battery state estimation approach: State-of-Energy. *Appl. Energy* **2015**, *151*, 41–48. [[CrossRef](#)]
49. Zhai, G.; Liu, S.; Wang, Z.; Zhang, W.; Ma, Z. State of Energy Estimation of Lithium Titanate Battery for Rail Transit Application. *Energy Procedia* **2017**, *105*, 3146–3151. [[CrossRef](#)]
50. Waag, W.; Fleischer, C.; Sauer, D.U. Adaptive on-line prediction of the available power of lithium-ion batteries. *J. Power Sources* **2013**, *242*, 548–559. [[CrossRef](#)]

51. Plett, G.L. Extended Kalman filtering for battery management systems of LiPB-based HEV battery packs: Part 1. Background. *J. Power Sources* **2004**, *134*, 252–261. [[CrossRef](#)]
52. Hu, X.; Li, S.; Peng, H.; Sun, F. Robustness analysis of State-of-Charge estimation methods for two types of Li-ion batteries. *J. Power Sources* **2012**, *217*, 209–219. [[CrossRef](#)]
53. Lim, K.; Bastawrous, H.A.; Duong, V.-H.; See, K.W.; Zhang, P.; Dou, S.X. Fading Kalman filter-based real-time state of charge estimation in LiFePO₄ battery-powered electric vehicles. *Appl. Energy* **2016**, *169*, 40–48. [[CrossRef](#)]
54. Gao, Z.C.; Chin, C.S.; Toh, W.D.; Chiew, J.; Jia, J. State-of-charge estimation and active cell pack balancing design of lithium battery power system for smart electric vehicle. *J. Adv. Transp.* **2017**, *2017*, 1–14. [[CrossRef](#)]
55. Jia, J.; Lin, P.; Chin, C.S.; Toh, W.D.; Gao, Z.; Lyu, H.; Cham, Y.T.; Mesbahi, E. Multirate strong tracking extended Kalman filter and its implementation on lithium iron phosphate (LiFePO₄) battery system. In Proceedings of the IEEE International Conference on Power Electronics and Drive Systems, Sydney, NSW, Australia, 9–12 June 2015; pp. 640–645.
56. Tang, X.; Liu, B.; Gao, F.; Lv, Z. State-of-charge estimation for Li-Ion power batteries based on a tuning free observer. *Energies* **2016**, *9*, 675. [[CrossRef](#)]
57. Torai, S.; Nakagomi, M.; Yoshitake, S.; Yamaguchi, S.; Oyama, N. State-of-health estimation of LiFePO₄/graphite batteries based on a model using differential capacity. *J. Power Sources* **2016**, *306*, 62–69. [[CrossRef](#)]
58. Ning, B.; Xu, J.; Cao, B.; Wang, B.; Xu, G. A sliding mode bbserver SOC estimation method based on parameter adaptive battery model. *Energy Procedia* **2016**, *88*, 619–626. [[CrossRef](#)]
59. Zhong, Q.; Zhong, F.; Cheng, J.; Li, H.; Zhong, S. State of charge estimation of lithium-ion batteries using fractional order sliding mode observer. *ISA Trans.* **2017**, *66*, 448–459. [[CrossRef](#)] [[PubMed](#)]
60. Kim, I.S. The novel state of charge estimation method for lithium battery using sliding mode observer. *J. Power Sources* **2006**, *163*, 584–590. [[CrossRef](#)]
61. Ma, Y.; Li, B.; Xie, Y.; Chen, H. Estimating the State of Charge of Lithium-ion Battery based on Sliding Mode Observer. *IFAC PapersOnLine* **2016**, *49*, 54–61. [[CrossRef](#)]
62. Zhang, F.; Liu, G.; Fang, L. A battery state of charge estimation method using sliding mode observer. In Proceedings of the 2008 World Congress on Intelligent Control and Automation, Chongqing, China, 25–27 June 2008; pp. 989–994.
63. Du, J.; Liu, Z.; Wang, Y.; Wen, C. An adaptive sliding mode observer for lithium-ion battery state of charge and state of health estimation in electric vehicles. *Control Eng. Pract.* **2016**, *54*, 81–90. [[CrossRef](#)]
64. Lin, C.; Mu, H.; Xiong, R.; Shen, W. A novel multi-model probability battery state of charge estimation approach for electric vehicles using H-infinity algorithm. *Appl. Energy* **2016**, *166*, 76–83. [[CrossRef](#)]
65. Mu, H.; Xiong, R.; Sun, F. A novel multi-model probability based battery state-of-charge fusion estimation approach. *Energy Procedia* **2016**, *88*, 840–846. [[CrossRef](#)]
66. Zhang, F.; Liu, G.; Fang, L.; Wang, H. Estimation of battery state of charge with H_{oo} observer: Applied to a robot for inspecting power transmission lines. *IEEE Trans. Ind. Electron.* **2012**, *59*, 1086–1095. [[CrossRef](#)]
67. Yan, J.; Xu, G.; Xu, Y.; Xie, B. Battery state-of-charge estimation based on H_{oo} filter for hybrid electric vehicle. In Proceedings of the International Conference on Control, Automation, Robotics and Vision, Hanoi, Vietnam, 17–20 December 2008; pp. 464–469.
68. Hu, X.; Sun, F.; Zou, Y. Estimation of State of Charge of a Lithium-Ion Battery Pack for Electric Vehicles Using an Adaptive Luenberger Observer. *Energies* **2010**, *3*, 1586–1603. [[CrossRef](#)]
69. Tsang, K.M.; Sun, L.; Chan, W.L. Identification and modelling of Lithium ion battery. *Energy Convers. Manag.* **2010**, *51*, 2857–2862. [[CrossRef](#)]
70. Wang, Q.; Jiang, B.; Li, B.; Yan, Y. A critical review of thermal management models and solutions of lithium-ion batteries for the development of pure electric vehicles. *Renew. Sustain. Energy Rev.* **2016**, *64*, 106–128. [[CrossRef](#)]
71. Panchal, S.; Mathewson, S.; Fraser, R.; Culham, R.; Fowler, M. Experimental measurements of thermal characteristics of LiFePO₄ battery. *SAE Tech. Pap.* **2015**, *2015*, 01–1189.
72. Panchal, S. *Impact of Vehicle Charge and Discharge Cycles on the Thermal Characteristics of Lithium-Ion Batteries*; UWSpace: Waterloo, ON, Canada, 2014; pp. 1–10.
73. Lu, L.; Han, X.; Li, J.; Hua, J.; Ouyang, M. A review on the key issues for lithium-ion battery management in electric vehicles. *J. Power Sources* **2013**, *226*, 272–288. [[CrossRef](#)]

74. Madani, S.; Schaltz, E.; Kær, S.K. Review of parameter determination for thermal modeling of lithium ion batteries. *Batteries* **2018**, *4*, 20. [[CrossRef](#)]
75. Heyer, B.F.W. One Meter Battery Tester. U.S. Patent 2,225,051 A, 16 May 1938.
76. Finger, E.P.; Marwell, E.M. Battery Control System for Battery Operated Vehicles. U.S. Patent 4,012,681, 3 January 1975.
77. Peled, E.; Yamin, H.; Reshef, I.; Kelrich, D.; Rozen, S. Method and Apparatus for Determining the State-of-Charge of Batteries Particularly Lithium Batteries. U.S. Patent 4,725,784 A, 16 February 1988.
78. Aylor, J.H.; Thieme, A.; Johnso, B.W. A battery state-of-charge indicator for electric wheelchairs. *IEEE Trans. Ind. Electron.* **1992**, *39*, 398–409. [[CrossRef](#)]
79. Rard, O.; Patillon, J.N.; D’Alch Buc, F. Neural network adaptive modeling of battery discharge behavior. In Proceedings of the International Conference on Artificial Neural Networks, Lausanne, Switzerland, 8–10 October 1997; pp. 1095–1100.
80. Jossen, A.; Spath, V.; Doring, H.; Garche, J. Battery management systems (BMS) for increasing battery life time. In Proceedings of the International Telecommunication Energy Conference, Dresden, Germany, 10 May 2000; p. 6.
81. Tian, X.; Jeppesen, B.; Ikushima, T.; Baronti, F.; Morello, R. Accelerating state-of-charge estimation in FPGA-based Battery Management Systems. In Proceedings of the Hybrid and Electric Vehicles Conference, London, UK, 2–3 November 2016; pp. 4–6.
82. Zhang, C.; Li, K.; Pei, L.; Zhu, C. An integrated approach for real-time model-based state-of-charge estimation of lithium-ion batteries. *J. Power Sources* **2015**, *283*, 24–36. [[CrossRef](#)]
83. Zheng, Y.; Ouyang, M.; Han, X.; Lu, L.; Li, J. Investigating the error sources of the online state of charge estimation methods for lithium-ion batteries in electric vehicles. *J. Power Sources* **2018**, *377*, 161–188. [[CrossRef](#)]
84. Long, X.; Wang, J.; Chen, Q. Kalman filtering state of charge estimation for battery management system based on a stochastic fuzzy neural network battery model. *Energy Convers. Manag.* **2012**, *53*, 33–39.
85. Waag, W.; Sauer, D.U. Adaptive estimation of the electromotive force of the lithium-ion battery after current interruption for an accurate state-of-charge and capacity determination. *Appl. Energy* **2013**, *111*, 416–427. [[CrossRef](#)]
86. Ting, T.O.; Man, K.L.; Lim, E.G.; Leach, M. Tuning of Kalman filter parameters via genetic algorithm for state-of-charge estimation in battery management system. *Sci. World J.* **2014**, *2014*, 176052. [[CrossRef](#)] [[PubMed](#)]
87. Yatsui, M.W.; Bai, H. Kalman filter based state-of-charge estimation for lithium-ion batteries in hybrid electric vehicles using pulse charging. In Proceedings of the Vehicle Power and Propulsion Conference, Chicago, IL, USA, 6–9 September 2011; pp. 1–5.
88. Zhang, R.; Cao, L.; Bao, S.; Tan, J. A method for connected vehicle trajectory prediction and collision warning algorithm based on V2V communication. *Int. J. Crashworth.* **2017**, *22*, 15–25. [[CrossRef](#)]
89. Wei, J.; Dong, G.; Chen, Z. On-board adaptive model for state of charge estimation of lithium-ion batteries based on Kalman filter with proportional integral-based error adjustment. *J. Power Sources* **2017**, *365*, 308–319. [[CrossRef](#)]
90. Hu, C.; Youn, B.D.; Chung, J. A multiscale framework with extended Kalman filter for lithium-ion battery SOC and capacity estimation. *Appl. Energy* **2012**, *92*, 694–704. [[CrossRef](#)]
91. Xiong, B.; Zhao, J.; Wei, Z.; Skyllas-Kazacos, M. Extended Kalman filter method for state of charge estimation of vanadium redox flow battery using thermal-dependent electrical model. *J. Power Sources* **2014**, *262*, 50–61. [[CrossRef](#)]
92. Yang, F.; Xing, Y.; Wang, D.; Tsui, K.-L. A comparative study of three model-based algorithms for estimating state-of-charge of lithium-ion batteries under a new combined dynamic loading profile. *Appl. Energy* **2016**, *164*, 387–399. [[CrossRef](#)]
93. Di Domenico, D.; Prada, E.; Creff, Y. An adaptive strategy for Li-ion battery internal state estimation. *Control Eng. Pract.* **2013**, *21*, 1851–1859. [[CrossRef](#)]
94. Wei, Z.; Tseng, K.J.; Wai, N.; Lim, T.M.; Skyllas-Kazacos, M. Adaptive estimation of state of charge and capacity with online identified battery model for vanadium redox flow battery. *J. Power Sources* **2016**, *332*, 389–398. [[CrossRef](#)]

95. Xiong, R.; Gong, X.; Mi, C.C.; Sun, F. A robust state-of-charge estimator for multiple types of lithium-ion batteries using adaptive extended Kalman filter. *J. Power Sources* **2013**, *243*, 805–816. [[CrossRef](#)]
96. Lee, S.J.; Kim, J.H.; Lee, J.M.; Cho, B.H. The state and arameter estimation of an Li-Ion battery using a new OCV-SOC concept. In Proceedings of the 2007 Power Electronics Specialists Conference, Orlando, FL, USA, 17–21 June 2007; pp. 2799–2803.
97. Chen, Z.; Fu, Y.; Mi, C.C. State of charge estimation of lithium-ion batteries in electric drive vehicles using extended kalman filtering. *IEEE Trans. Veh. Technol.* **2013**, *62*, 1020–1030. [[CrossRef](#)]
98. Zhu, Z.; Sun, J.; Liu, D. Online state of charge EKF estimation for LiFePO₄ battery management systems. In Proceedings of the International Symposium on Intelligent Signal Processing and Communications Systems, Taipei, Taiwan, 4–7 November 2012; pp. 609–614.
99. He, H.; Liu, Z.; Hua, Y. Adaptive extended kalman filter based fault detection and isolation for a lithium-ion battery pack. *Energy Procedia* **2015**, *75*, 1950–1955. [[CrossRef](#)]
100. Xiong, R.; He, H.; Sun, F.; Zhao, K. Evaluation on state of charge estimation of batteries with adaptive extended kalman filter by experiment approach. *IEEE Trans. Veh. Technol.* **2013**, *62*, 108–117. [[CrossRef](#)]
101. Zheng, F.; Xing, Y.; Jiang, J.; Sun, B.; Kim, J.; Pecht, M. Influence of different open circuit voltage tests on state of charge online estimation for lithium-ion batteries. *Appl. Energy* **2016**, *183*, 513–525. [[CrossRef](#)]
102. Xing, Y.; He, W.; Pecht, M.; Tsui, K.L. State of charge estimation of lithium-ion batteries using the open-circuit voltage at various ambient temperatures. *Appl. Energy* **2014**, *113*, 106–115. [[CrossRef](#)]
103. Plett, G.L. Sigma-point Kalman filtering for battery management systems of LiPB-based HEV battery packs: Part 1: Introduction and state estimation. *J. Power Sources* **2006**, *161*, 1356–1368. [[CrossRef](#)]
104. Plett, G.L. Sigma-point Kalman filtering for battery management systems of LiPB-based HEV battery packs: Part 2: Simultaneous state and parameter estimation. *J. Power Sources* **2006**, *161*, 1369–1384. [[CrossRef](#)]
105. He, Z.; Liu, Y.; Gao, M.; Wang, C. A joint model and SOC estimation method for lithium battery based on the sigma point KF. In Proceedings of the Transportation Electrification Conference and Expo, Dearborn, MI, USA, 18–20 June 2012; pp. 1–5.
106. Xia, B.; Sun, Z.; Zhang, R.; Lao, Z.; Xia, B.; Sun, Z.; Zhang, R.; Lao, Z. A cubature particle filter algorithm to estimate the state of the charge of lithium-ion batteries based on a second-order equivalent circuit model. *Energies* **2017**, *10*, 457. [[CrossRef](#)]
107. Ye, M.; Guo, H.; Xiong, R.; Yu, Q. A double-scale and adaptive particle filter-based online parameter and state of charge estimation method for lithium-ion batteries. *Energy* **2018**, *144*, 789–799. [[CrossRef](#)]
108. Charkhgard, M.; Zarif, M.H. Design of adaptive Hoo filter for implementing on state-of-charge estimation based on battery state-of-charge-varying modelling. *Power Electron. IET* **2015**, *8*, 1825–1833. [[CrossRef](#)]
109. Xia, B.; Cui, D.; Sun, Z.; Lao, Z.; Zhang, R.; Wang, W.; Sun, W.; Lai, Y.; Wang, M. State of charge estimation of lithium-ion batteries using optimized Levenberg-Marquardt wavelet neural network. *Energy* **2018**, *153*, 694–705. [[CrossRef](#)]
110. Dang, X.; Yan, L.; Xu, K.; Wu, X.; Jiang, H.; Sun, H. Open-circuit voltage-based state of charge estimation of lithium-ion battery using dual neural network fusion battery model. *Electrochim. Acta* **2016**, *188*, 356–366. [[CrossRef](#)]
111. Tong, S.; Lacap, J.H.; Park, J.W. Battery state of charge estimation using a load-classifying neural network. *J. Energy Storage* **2016**, *7*, 236–243. [[CrossRef](#)]
112. Chaoui, H.; Ibe-Ekeocha, C.C.; Gualous, H. Aging prediction and state of charge estimation of a LiFePO₄ battery using input time-delayed neural networks. *Electr. Power Syst. Res.* **2017**, *146*, 189–197. [[CrossRef](#)]
113. Hu, J.N.; Hu, J.J.; Lin, H.B.; Li, X.P.; Jiang, C.L.; Qiu, X.H.; Li, W.S. State-of-charge estimation for battery management system using optimized support vector machine for regression. *J. Power Sources* **2014**, *269*, 682–693. [[CrossRef](#)]
114. Sheng, H.; Xiao, J. Electric vehicle state of charge estimation: Nonlinear correlation and fuzzy support vector machine. *J. Power Sources* **2015**, *281*, 131–137. [[CrossRef](#)]
115. Blaifi, S.; Moulahoum, S.; Colak, I.; Merrouche, W. An enhanced dynamic model of battery using genetic algorithm suitable for photovoltaic applications. *Appl. Energy* **2016**, *169*, 888–898. [[CrossRef](#)]
116. Xu, J.; Cao, B.; Chen, Z.; Zou, Z. An online state of charge estimation method with reduced prior battery testing information. *Int. J. Electr. Power Energy Syst.* **2014**, *63*, 178–184. [[CrossRef](#)]
117. Chen, Z.; Mi, C.C.; Fu, Y.; Xu, J.; Gong, X. Online battery state of health estimation based on Genetic Algorithm for electric and hybrid vehicle applications. *J. Power Sources* **2013**, *240*, 184–192. [[CrossRef](#)]

118. Gao, Z.; Cheng, S.C.; Woo, W.L.; Jia, J.; Wei, D.T. Genetic algorithm based back-propagation neural network approach for fault diagnosis in lithium-ion battery system. In Proceedings of the International Conference on Power Electronics Systems and Applications, Hong Kong, China, 15–17 December 2015; pp. 1–6.
119. Awadallah, M.A.; Venkatesh, B. Accuracy improvement of SOC estimation in lithium-ion batteries. *J. Energy Storage* **2016**, *6*, 95–104. [CrossRef]
120. Cai, C.H.; Du, D.; Liu, Z.Y. Battery state-of-charge (SOC) estimation using adaptive neuro-fuzzy inference system (ANFIS). In Proceedings of the IEEE International Conference on Fuzzy Systems, St Louis, MO, USA, 25–28 May 2003; Volume 1062, pp. 1068–1073.
121. Affanni, A.; Bellini, A.; Concari, C.; Franceschini, G. EV battery state of charge: Neural network based estimation. In Proceedings of the IEEE International Electric Machines and Drives Conference, IEMDC'03, Madison, WI, USA, 1–4 June 2003; Volume 682, pp. 684–688.
122. Zhou, F.; Wang, L.; Lin, H.; Lv, Z. High accuracy state-of-charge online estimation of EV/HEV lithium batteries based on Adaptive Wavelet Neural Network. In Proceedings of the Ecce Asia Downunder, Melbourne, VIC, Australia, 3–6 June 2013; pp. 513–517.
123. Dai, H.; Guo, P.; Wei, X.; Sun, Z.; Wang, J. ANFIS (Adaptive Neuro-Fuzzy Inference System) based online SOC (State of Charge) correction considering cell divergence for the EV (Electric Vehicle) traction batteries. *Energy* **2015**, *80*, 350–360. [CrossRef]
124. Tian, Y.; Li, D.; Tian, J.; Xia, B. State of charge estimation of lithium-ion batteries using an optimal adaptive gain nonlinear observer. *Electrochim. Acta* **2017**, *225*, 225–234. [CrossRef]
125. Tang, X.; Wang, Y.; Chen, Z. A method for state-of-charge estimation of LiFePO₄ batteries based on a dual-circuit state observer. *J. Power Sources* **2015**, *296*, 23–29. [CrossRef]
126. Xia, B.; Chen, C.; Tian, Y.; Sun, W.; Xu, Z.; Zheng, W. A novel method for state of charge estimation of lithium-ion batteries using a nonlinear observer. *J. Power Sources* **2014**, *270*, 359–366. [CrossRef]
127. Ma, Y.; Li, B.; Li, G.; Zhang, J.; Chen, H. A nonlinear observer approach of SOC estimation based on hysteresis model for lithium-ion battery. *IEEE/CAA J. Autom. Sin.* **2017**, *4*, 195–204. [CrossRef]
128. Xu, J.; Mi, C.C.; Cao, B.; Deng, J. The state of charge estimation of lithium-ion batteries based on a proportional-integral observer. *IEEE Trans. Veh. Technol.* **2014**, *63*, 1614–1621.
129. Kim, I.S. Nonlinear state of charge estimator for hybrid electric vehicle battery. *IEEE Trans. Power Electron.* **2008**, *23*, 2027–2034.
130. Xia, B.; Zheng, W.; Zhang, R.; Lao, Z.; Sun, Z.; Sciubba, E. A novel observer for lithium-ion battery state of charge estimation in electric vehicles based on a second-order equivalent circuit model. *Energies* **2017**, *10*, 1150. [CrossRef]
131. Wang, Q.; Wang, J.; Zhao, P.; Kang, J.; Yan, F.; Du, C. Correlation between the model accuracy and model-based SOC estimation. *Electrochim. Acta* **2017**, *228*, 146–159. [CrossRef]
132. Meng, J.; Luo, G.; Gao, F. Lithium polymer battery state-of-charge estimation based on adaptive unscented kalman filter and support vector machine. *IEEE Trans. Power Electron.* **2016**, *31*, 2226–2238. [CrossRef]
133. Cheng, K.W.E.; Divakar, B.P.; Wu, H.; Ding, K.; Ho, H.F. Battery-Management System (BMS) and SOC Development for Electrical Vehicles. *IEEE Trans. Veh. Technol.* **2011**, *60*, 76–88. [CrossRef]
134. Unterrieder, C.; Priewasser, R.; Marsili, S.; Huemer, M. Battery state estimation using mixed kalman/hinfinity, adaptive luenberger and sliding mode observer. In Proceedings of the Vehicle Power and Propulsion Conference, Beijing, China, 15–18 October 2013; pp. 1–6.
135. Wang, L.; Wang, L.; Li, Y. A novel state-of-charge estimation algorithm of EV battery based on bilinear interpolation. In Proceedings of the Vehicle Power and Propulsion Conference, Beijing, China, 15–18 October 2013; pp. 1–4.
136. Lavigne, L.; Sabatier, J.; Francisco, J.M.; Guillemard, F.; Noury, A. Lithium-ion open circuit voltage (OCV) curve modelling and its ageing adjustment. *J. Power Sources* **2016**, *324*, 694–703. [CrossRef]
137. Xing, S.; Chen, S.; Wei, Z.; Xia, J. Unifying electrical engineering and electronics engineering: Proceedings of the 2012 international conference on electrical and electronics engineering. In *Lecture Notes in Electrical Engineering*; Springer: Berlin, Germany, 2014; Volume 238. [CrossRef]
138. Sun, F.; Xiong, R.; He, H. A systematic state-of-charge estimation framework for multi-cell battery pack in electric vehicles using bias correction technique. *Appl. Energy* **2016**, *162*, 1399–1409. [CrossRef]
139. Wu, C.; Zhu, C.; Ge, Y.; Zhao, Y. A review on fault mechanism and diagnosis approach for Li-Ion batteries. *J. Nanomater.* **2015**, *2015*, 8. [CrossRef]

140. Gold, L.; Bach, T.; Virsik, W.; Schmitt, A.; Müller, J.; Staab, T.E.M.; Sextl, G. Probing lithium-ion batteries' state-of-charge using ultrasonic transmission—Concept and laboratory testing. *J. Power Sources* **2017**, *343*, 536–544. [[CrossRef](#)]
141. Gallien, T.; Krenn, H.; Fischer, R.; Lauterbach, S.; Schweighofer, B.; Wegleiter, H. Magnetism versus LiFePO₄ battery's state of charge: A feasibility study for magnetic-based charge monitoring. *IEEE Trans. Instrum. Meas.* **2015**, *64*, 2959–2964. [[CrossRef](#)]
142. Cannarella, J.; Arnold, C.B. State of health and charge measurements in lithium-ion batteries using mechanical stress. *J. Power Sources* **2014**, *269*, 7–14. [[CrossRef](#)]
143. Gao, Z.; Chin, C.; Woo, W.; Jia, J. Integrated equivalent circuit and thermal model for simulation of temperature-dependent LiFePO₄ battery in actual embedded application. *Energies* **2017**, *10*, 85. [[CrossRef](#)]



© 2018 by the authors. Licensee MDPI, Basel, Switzerland. This article is an open access article distributed under the terms and conditions of the Creative Commons Attribution (CC BY) license (<http://creativecommons.org/licenses/by/4.0/>).